POLITECNICO DI TORINO
Repository ISTITUZIONALE

A Tutorial on Speckle Reduction in Synthetic Aperture Radar Images

Original
A Tutorial on Speckle Reduction in Synthetic Aperture Radar Images / Fabrizio, Argenti; Alessandro, Lapini; Bianchi, Tiziano; Luciano, Alparone. - In: IEEE GEOSCIENCE AND REMOTE SENSING MAGAZINE. - ISSN 2168-6831. - 1:3(2013), pp. 6-35. [10.1109/MGRS.2013.2277512]

Availability:
This version is available at: 11583/2515888 since:

Publisher:
IEEE - INST ELECTRICAL ELECTRONICS ENGINEERS INC

Published
DOI:10.1109/MGRS.2013.2277512

Terms of use:

This article is made available under terms and conditions as specified in the corresponding bibliographic description in the repository

Publisher copyright

(Article begins on next page)

12 October 2024

A Tutorial on Speckle Reduction in Synthetic Aperture Radar Images

Fabrizio Argenti, *Senior Member, IEEE,* Alessandro Lapini, *Student Member, IEEE,* Tiziano Bianchi, *Member, IEEE,* and Luciano Alparone

***Abstract*—Speckle is a granular disturbance, usually modeled as a multiplicative noise, that affects synthetic aperture radar (SAR) images, as well as all *coherent* images. Over the last three decades, several methods have been proposed for the reduction of speckle, or *despeckling*, in SAR images. Goal of this paper is making a comprehensive review of despeckling methods since their birth, over thirty years ago, highlighting trends and changing approaches over years. The concept of fully developed speckle is explained. Drawbacks of homomorphic filtering are pointed out. Assets of multiresolution despeckling, as opposite to spatial-domain despeckling, are highlighted. Also advantages of undecimated, or stationary, wavelet transforms over decimated ones are discussed. Bayesian estimators and probability density function (pdf) models in both spatial and multiresolution domains are reviewed. Scale-space varying pdf models, as opposite to scale varying models, are promoted. Promising methods following non-Bayesian approaches, like nonlocal (NL) filtering and total variation (TV) regularization, are reviewed and compared to spatial- and wavelet-domain Bayesian filters. Both established and new trends for assessment of despeckling are presented. A few experiments on simulated data and real COSMO-SkyMed SAR images highlight, on one side the cost-performance trade-off of the different methods, on the other side the effectiveness of solutions purposely designed for SAR heterogeneity and not fully developed speckle. Eventually, upcoming methods based on new concepts of signal processing, like compressive sensing, are foreseen as a new generation of despeckling, after spatial-domain and multiresolution-domain methods.**

I. Introduction

SYNTHETIC aperture radar (SAR) remote sensing [1] offers a number of advantages over optical remote sensing, mainly the all-day, all-weather acquisition capability. However, the main drawback of SAR images is the presence of *speckle*, a signal dependent granular noise, inherent of all active coherent imaging systems, that visually degrades the appearance of images. Speckle may severely diminish the performances of automated scene analysis and information extraction techniques, as well as it may be harmful in applications requiring multiple SAR observations, like automatic multitemporal change detection. For these reasons, a preliminary processing of real-valued detected SAR images aimed at speckle reduction, or *despeckling*, is of crucial importance for a number of applications. Such a preprocessing, however, should be carefully designed to avoid spoiling useful information, such as local mean of backscatter, point targets, linear features and textures.

A steadily increasing number of papers specific on despeckling has appeared in the literature over the last ten years, presumably because the new generation of satellite SAR systems has dramatically raised the attention of researchers in signal processing towards this problem. The COSMO-SkyMed constellation - four satellites launched by the Italian Space Agency (ASI) between 2007 and 2010 - features X-band SAR with low revisit-time; as a second generation mission, two additional satellites are foreseen in 2014 and 2015. The twin-satellite constellation TerraSAR-X / TanDem-X (2007 / 2010) launched by the German Space Agency (DLR) and the upcoming Sentinel-1a / -1b satellite constellation (2013 / 2015) from the European Space Agency (ESA), which shall extend the EnviSat mission, complete the European scenario of satellite SAR. Also, the Canadian RADARSAT 3 mission is expected in a near future, with 3 satellites operating at C-band, to be launched in 2017. A thorough overview of past, present and future missions can be found in [1].

The most recent advances in despeckling pursue the technological objective of giving an extra value to the huge amount of data that are routinely collected by current and upcoming SAR systems mounted on orbiting platforms. In fact, with the exception of applications related to production of digital elevation models (DEMs) or interferometric phase maps useful for studies of terrain deformation (landslides, subsidence, etc.), SAR data do not find the same full utilization, as optical data do, by either users' or scientists' communities. As an example, the functional development of efficient techniques for fusion between optical and SAR data would constitute an enabling technology that would allow a relevant number of new applications to bring benefits both for data providers and for producers of software applications. Unfortunately, speckle is the main obstacle towards the development of an effective optical-SAR fusion [2], together with the different acquisition geometry of optical and SAR systems.

This article is intended as tutorial on despeckling, rather than a simple review of despeckling methods. Therefore, emphasis is given to speckle and reflectivity models that are used for filtering. The review of methods that are not relying on the multiplicative noise model is kept very concise, since such methods have not encountered same progresses over time

This work has been carried out under the financial support of Italian Space Agency (ASI), COSMO-Skymed AO ID #2293.

Copyright (c) 2013 IEEE. Personal use of this material is permitted. However, permission to use this material for any other purposes must be obtained from the IEEE by sending a request to pubs-permissions@ieee.org

Fabrizio Argenti, Alessandro Lapini and Luciano Alparone are with the Department of Information Engineering, University of Florence, Via S. Marta, 3, 50139 Florence, Italy (e-mail: fabrizio.argenti@unifi.it, alessandro.lapini@unifi.it, alparone@iapp.det.unifi.it).

T. Bianchi is with the Department of Electronics and Telecommunications, Politecnico di Torino, Corso Duca degli Abruzzi, 24, 10129 Torino, Italy (e-mail: tiziano.bianchi@polito.it).

as model-based methods have. With only very few exception, despeckling methods specifically proposed for ultrasound images are not reviewed here. In fact, notwithstanding the similarity of the coherent imaging system, in the presence of weak echoes from tissues the additive white Gaussian noise (AWGN) introduced by the electronics cannot be neglected and the noise model also includes an AWGN term [3]. In SAR images, the AWGN term is always negligible, compared to the signal-dependent term [4].

Despeckling methods specifically pertaining to *polarimetric* SAR are not discussed in this tutorial. Readers interested to this topic are addressed to the seminal papers by Novak and Burl [5], Lee *et al.* [6] and Touzi and Lopès [7], as well as to more recent and developed contributions [8], [9]. Also despeckling methods designed to take advantage of the availability of a temporal sequence of SAR images, like [10], [11], are not addressed here. By default, speckle reduction is approached as *mono-variate*, even though a *multivariate* speckle reduction [12], if applicable, may be preferred.

Only *incoherent* processing, that is, processing of SAR images in either power, referred to as *intensity*, or amplitude formats is dealt with. In fact, *coherent* processing of data in complex format does not increase the signal-to-noise ratio (SNR), but only the *coherence* [13] of the interferogram and thus it is used in SAR interferometry [14]. The noisy phase of the complex interferogram may be filtered before it is unwrapped [15], [16], but in many cases the regularization is directly performed by the unwrapping algorithm [17]. Whenever two real valued detected SAR images of the same scene are available, the temporal correlation of speckle conveys information on the coherence of the interferogram that would be calculated from complex data [18]. Thus, speckle is not only noise but in some sense has an information content, even if difficult to exploit.

Excellent reviews of despeckling methods with high tutorial value have been written by Lee *et al.* [19] and Touzi [20]. Our goal is to update the presentation of methods to changing times, especially towards recently established concepts of multiresolution processing. A brief perspective on upcoming promising approaches to despeckling in particular, and to information extraction from SAR images in general, is also included in this survey.

The organization of contents is the following. After a leisurely paced section on fundamentals of reflectivity, speckle and imaging system modeling, the problem is addressed and developed under a statistical signal processing perspective, as in [20]. Emphasis is given to Bayesian estimation in either space or scale-space domains. The main features of the latter are concisely surveyed. A comprehensive critical review of the most relevant speckle filters, beginning with the pioneering Lee filter [21], spans over thirty years and highlights trends and fashions that have been pursued and developed over time or quickly abandoned. The renewed interest of researchers towards despeckling occurred with the introduction of multiresolution analysis, when spatial domain methods had reached a degree of sophistication, together with a saturation of performances, that demanded a cross-fertilization from other fields of signal processing. A variety of wavelet-based, or more generally scale-space, despeckling methods is contextualized and discussed. Advantages of such methods over spatial domain methods is pointed out. Promising approaches like nonlocal filtering and total variation regularization are described.

The second part of the article contains a more articulated review of a few selected methods, some of them recently proposed by the authors, that are presently indicated as highly performing [22] in a comparative assessment carried out on image specimens produced by a SAR simulator [23]. The most established and widely used statistical indexes to assess the quality of despeckling, both with a reference, like in the case of the SAR simulator, or of synthetically speckled optical images, and *blind*, i.e., without a reference, are surveyed. A brief section compares quantitative results of the selected methods and draws some considerations on the specific features of the different methods, which exhibit different behaviors, and on the suitability and limitations of the quality indexes. The trade off between performances and computational cost is analyzed. The influence of speckle correlation on the despeckling accuracy of single-look images and a viable strategy for its preliminary reduction, without affecting the subsequent despeckling stages, is described. Eventually, a concluding section remarks the key points of the analysis and gives hints that may help researchers develop new and better despeckling filters, or more simply may help users choose the most suitable filter among those that are presently available, also as source or executable codes to download.

II. Signal and Noise Modeling

Under a statistical signal processing perspective, despeckling filters aim at estimating the noise-free radar reflectivity from the observed noisy SAR image [20]. In order to describe the estimation methods that have been developed for the despeckling problem, we need firstly to introduce models for speckle, SAR system and reflectivity.

A. Speckle models

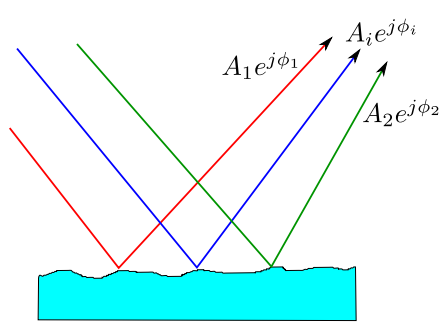

Fig. 1. Scattering model explaining fully developed speckle.

SAR is an active acquisition instrument that produces a radiation and captures the signals backscattered from a small area of the imaged scene (*resolution cell*). The received signal, as output from the in-phase and quadrature channels, is complex. If we assume that the resolution cell contains several scatterers and that no one yields a reflected signal

much stronger than the others (*distributed target*), then the received signal can be viewed as the incoherent sum of several backscattered waves, i.e., $Ae^{j\phi} = \sum_i A_i e^{j\phi_i}$, as shown in Fig. 1. The amplitudes A_i and phases ϕ_i are the results of several factors, including propagation attenuation, scattering of the illuminated targets, antenna directivity. Each individual component, however, can not be resolved within a resolution cell. A first approach to modeling the received signal is solving the Maxwell's equations according to the propagation geometry and scattering medium [24], [25]. By using this approach, the way each propagation path interferes gives us basic information about the observed scene. On the other hand, if we consider that the phases of each path are highly different and that they may sum in a constructive or destructive way, then the amplitude of the received signal varies randomly. So, even if the underlying reflectivity field is uniform, it appears as affected by a "granular" noise after the imaging system. For visual inspection and for specific applications that involve visual information retrieval, such as mapping and segmentation, the highly varying nature of the signal may be considered as a disturbance and is commonly denoted as "speckle".

The phases ϕ_i are highly varying (since the wavelength is much shorter than the resolution cell size and scatterers distances) and may be considered as uniformly distributed in $(-\pi, \pi)$ as well as independent of A_i. If the number of scatterers is sufficiently high, the central limit theorem applies [26] and the resulting signal $Ae^{j\phi} = z_1 + jz_2$ can be seen as a complex signal whose real and imaginary parts (in-phase and quadrature components) are independent and identically distributed zero-mean Gaussian variables with variance $\sigma/2$. When this applies speckle is termed as *fully developed* [27]. The joint probability density function (pdf) is given by

$$p_{z_1,z_2}(z_1, z_2) = \frac{1}{\pi\sigma} e^{-\frac{z_1^2+z_2^2}{\sigma}} \tag{1}$$

whereas the amplitude A is distributed as a Rayleigh pdf, that is

$$p_A(A) = \frac{2A}{\sigma} e^{-\frac{A^2}{\sigma}} \tag{2}$$

and the power or *intensity* $I = A^2$ is distributed according to an exponential pdf, that is

$$p_I(I) = \frac{1}{\sigma} e^{-\frac{I}{\sigma}} \tag{3}$$

so that the mean of the intensity is equal to σ. It can be shown [4], [28] that the intensity measurement carries information about the average backscattering coefficient (for distributed targets) related to the resolution cell. Hence, for specific applications, the parameter σ is the actual information we would like to extract from a single channel SAR system. This can be considered as the radar cross section (RCS) of the observed resolution cell. The received signal pdf can be reformulated into

$$p_{I|\sigma}(I|\sigma) = \frac{1}{\sigma} e^{-\frac{I}{\sigma}} \tag{4}$$

or

$$I = \sigma u \tag{5}$$

where u is exponentially distributed, that is,

$$p_u(u) = e^{-u} \tag{6}$$

Eq. (5) is termed the *multiplicative model* of speckle.

If only one image (realization of the stochastic process) is available, the best estimate of the scene average reflectivity is just the pixel-by-pixel intensity. This will be a quite noisy estimate because of the previously described constructive/destructive combination effects. From (3), it follows that the variance of the intensity in each pixel is σ^2, so that brighter pixel will be affected by stronger disturbances than darker ones. A way to improve the estimation of σ is to average L independent intensity values related to the same position. This processing, named "multilooking", maintains the mean intensity σ but reduces the estimator variance to σ^2/L. Independent "looks" of a target resolution cell can be obtained either by appropriate processing in the Doppler domain (splitting the Doppler bandwidth within the imaging system that compensates the quadratic phase variation created by the platform movement) or by averaging L spatial observations. In both cases, the cost to be paid for estimation accuracy improvement is spatial resolution loss by a factor L. If the hypothesis of independent intensity measurements holds (in the case of correlated data the assumption fails), the L-look averaged intensity I_L is Γ-distributed, that is

$$p_{I_L|\sigma}(I_L|\sigma) = \frac{1}{\Gamma(L)} \left(\frac{L}{\sigma}\right)^L {I_L}^{L-1} e^{-\frac{LI_L}{\sigma}} \tag{7}$$

whereas the relative amplitude image $A_L = \sqrt{I_L}$ has a square-root Γ distribution [4]. For visual inspection and for automatic interpretation tasks, the use of amplitude images is preferable, thanks to their reduced dynamic range with respect to intensity images, which is accompanied by an increment in SNR.

The model described above is valid under the assumption that the imaged scene is characterized by distributed scatterers. In the presence of a scatterer much stronger than the others (*point target*), the received signal pdf becomes a Rice distribution and the model above described does not apply. In this case, the received signal power is related to the single target reflection coefficient and, for the purpose of speckle removal, point targets are treated separately from distributed targets.

B. SAR system model

In the above analysis, the effect of the imaging system has not been taken into consideration. Indeed, the SAR system can achieve a spatial resolution of the order of the antenna size only if proper processing, referred to as *focusing*, is applied. The energy of the transmitted frequency modulated (FM) chirp pulse is spread into the range-Doppler domain and such a processing consists of matched filtering along the range and along iso-Doppler curves and is needed to compact energy back in the spatial domain [28]. From this point of view, a SAR system can be seen as an encoding transfer function $h_e(\mathbf{r})$ followed by a compression transfer function $h_c(\mathbf{r})$ [4], [29]. If $S(\mathbf{r})$ denotes the complex reflectivity, the observed single look complex (SLC) signal after the imaging processor is

$$g_c(\mathbf{r}) = [C \cdot S(\mathbf{r}) * h_e(\mathbf{r}) + n(\mathbf{r})] * h_c(\mathbf{r}) \tag{8}$$

where the constant C absorbs propagation information (e.g., loss and antenna gains) and the term $n(\mathbf{r})$ accounts for thermal noise at the receiver. For sufficiently high signal-to-noise ratios, the noise term can be neglected and the received complex signal becomes

$$g_c(\mathbf{r}) = C \cdot S(\mathbf{r}) * h_e(\mathbf{r}) * h_c(\mathbf{r}) = C \cdot S(\mathbf{r}) * h(\mathbf{r}) \tag{9}$$

For well-designed SAR, the impulse response $h(\mathbf{r})$ is pulse-like and represents the point spread function (PSF) of the system that, in a first approximation, can be assumed as independent of the position. Again, the intensity $|g_c(\mathbf{r})|^2$ is proportional to the average backscattering coefficient of the cell and is the information we would like to achieve from the observation. An accurate description of the model in (9) and of the statistical properties of the acquired SAR image is given in [29].

C. Reflectivity models

The speckle formation model yields a pixelwise description of the observed signal. For many applications, including despeckling, more refined models are needed. Such models describe the observed received signal at a coarser scale than the single pixel one and try to intercept information about the underlying texture of the imaged scene and its correlation. It is then crucial to consider also the average intensity, i.e., RCS σ, which is considered the information to be retrieved, as a random process. Unfortunately, the RCS is not directly observable and its properties must be inferred from the intensity values over an area in which the texture is homogeneous. In this sense, RCS modeling can be seen as an inverse problem whose solution is made difficult by the fact that homogeneity can be stated only if a ground truth is available, but often this is not the case. Furthermore, since the problem can be formulated only in a statistical sense, the dimension of the homogeneous area becomes crucial: it should be as large as possible in order to reliably apply statistical hypothesis testing methods, but this contrasts with the natural scenes structure that is often characterized by the presence of limited size homogeneous areas (such as fields, woods, orchards, forests, trees, man-made areas) and mixing the information of different textures makes the hypothesis tests to fail.

The starting point for solving this inverse problem is the statistics of the observed intensity over a homogeneous area. The pdf of the intensity signal can be written as

$$p(I) = \int p(I|\sigma)p(\sigma)d\sigma \tag{10}$$

where $p(I|\sigma)$ is the single pixel speckle model, given by (4) and (7) for the 1-look and L-look cases, respectively. Eq. (10) is referred to as the *product model* of the observed intensity [20]. One of the assumptions that must be made to state the validity of the model (10) is that the RCS fluctuation scale is larger than that of speckle.

Even though several pdfs have been proposed for the intensity I (e.g., Weibull, log–normal), one of the most used pdf is the K distribution. The K distribution is a parametric pdf that, with a suitable choice of its parameters, well fits observed intensity histograms. It has also the advantage that a closed form of the RCS pdf, i.e., $p(\sigma)$, exists such that the product model in (10) yields a K distribution. In fact, if the RCS pdf is a Γ distribution, that is

$$p(\sigma) = \left(\frac{\nu}{\bar{\sigma}}\right)^{\nu} \frac{\sigma^{\nu-1}}{\Gamma(\nu)} e^{-\frac{\nu\sigma}{\bar{\sigma}}} \tag{11}$$

where ν is an *order* parameter and $\bar{\sigma}$ is the mean, then the pdf of the observed intensity signal is given by

$$p(I) = \frac{2}{\Gamma(L)\Gamma(\nu)} \left(\frac{L\nu}{\bar{I}}\right)^{\frac{L+\nu}{2}} I^{\frac{L+\nu-2}{2}} K_{\nu-L}\left(2\sqrt{\frac{\nu L I}{\bar{I}}}\right) \tag{12}$$

where $K_n(\cdot)$ is the modified Bessel function of order n and $\bar{I}$ is the mean of intensity. Fitting the parameters of the pdf to the observed signal allows information on the RCS to be retrieved.

The model in (12) yields a pixelwise statistical description of the observed intensity values. A complete description of the scene, however, needs the inclusion of the autocorrelation function into the model. If such a function is estimated from the observed data, then the exact autocorrelation function of the RCS is quite difficult to achieve and usually it does not exist in a closed form [4].

III. Space and Scale-Space Domain Estimation

From the previous discussion, it emerges that modeling the received SAR signal should take into account several physical, statistical and engineering aspects of the overall system. Such a complexity makes the process of extracting average backscatter information from the observed signal a nontrivial task. From a signal processing perspective, a first step towards finding efficient solutions is stating the acquisition model in the simplest form as possible. In [20], several multiplicative models of speckle are described and classified according to the autocorrelations of the imaged scene and of the noise term.

In the following of this section, models of the noisy signal in both spatial and transformed domains are reviewed, Bayesian estimation principles are briefly recalled and the wavelet transform, in both decimated and undecimated versions, is introduced as a transformation suitable for despeckling. Eventually, the modeling of pdfs for Bayesian estimation in the wavelet domain is discussed and shown to be crucial for performances.

A. Models of noisy signal

Perhaps, the most used model in the literature on despeckling is the following:

$$g = fu \tag{13}$$

where f is a possibly autocorrelated random process and represents the noise–free reflectivity; u is a possibly autocorrelated stationary random process, independent of f, and represents the speckle fading term; g is the observed noisy image. All the quantities in (13) may refer to either intensity or amplitude as well as to single-look or multilook images, whose pdfs have been described previously.

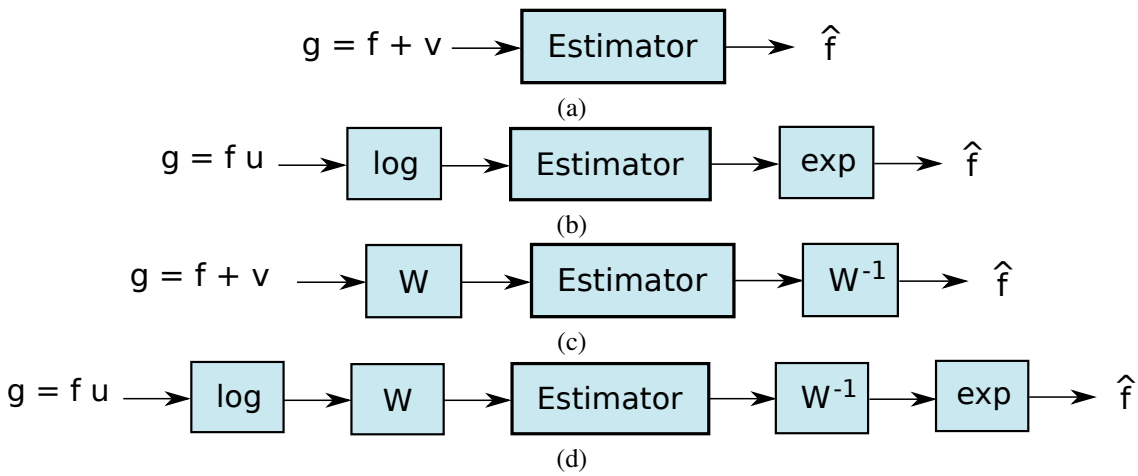

Fig. 2. Additive models commonly used in despeckling algorithms: (a) signal-dependent in spatial domain; (b) signal-independent in spatial domain; (c) signal-dependent in transform domain; (d) signal-independent in transform domain.

The variable u may be assumed as spatially correlated [30]. Recently, it has been shown [31] that a preprocessing step that makes speckle uncorrelated, that is "whitens" the complex signal, allows despeckling algorithms designed for uncorrelated speckle to be successfully applied also when speckle is (auto)correlated. Therefore, in the following we shall analyze only algorithms working under the hypothesis of uncorrelated speckle.

The nonlinear nature of the relationship between observed and noise-free signals makes the filtering procedure a non-trivial task. For this reason, some manipulations have been introduced to make the observation model simpler. Several authors adopt the following model, derived from (13):

$$g = f + (u-1)f = f + v, \tag{14}$$

where $v = (u-1)f$ accounts for speckle disturbance in an equivalent additive model, in which v, depending on f, is a *signal-dependent* noise process.

A second way that allows the multiplicative noise to be transformed into an additive one is using a *homomorphic* transformation [32]. It consists of taking the logarithm of the observed data, so that we have

$$\begin{aligned} \log g &= \log f + \log u \\ g' &= f' + u' \end{aligned} \tag{15}$$

where g', f' and u' denote the logarithm of the quantities in (13). Unlike the case in (14), here the noise component u' is a *signal-independent* additive noise. However, this operation may introduce a bias into the denoised image, since an unbiased estimation in the log-domain is mapped onto a biased estimation in the spatial domain [33]; in math form, if u exhibits $E[u] = 1$, $E[u'] = E[\log(u)] \neq \log(E[u]) = \log(1) = 0$.

Over the last two decades, approaches to image denoising that perform estimation in a transformed domain have been proposed. Transforms derived from multiresolution signal analysis [34], [35], such as the discrete wavelet transform (DWT), are the most popular in this context. Despeckling in a transform domain is carried out by taking the direct transform of the observed signal, by estimating the speckle-free coefficients and by reconstructing the filtered image through the inverse transform applied to the despeckled coefficients.

B. Bayesian estimation concepts

From the previous discussion about the most widely used signal models for despeckling, it can be seen that the multiplicative model is often manipulated in order to obtain an additive one. Fig. 2 summarizes the various versions of the additive models.

The block "Estimator" attempts to achieve a speckle-free representation of the signal in a specific domain; for example, in the transform domain, as in Fig. 2-(c), or in the homomorphic-transform domain, as in Fig. 2-(d), in which the noise-free informative signal is contaminated with additive signal-dependent or signal-independent noise, respectively.

The basics of Bayesian estimation are now reviewed for the simplest case, shown in Fig. 2-(a), even though analogous derivations hold for all the other cases in Fig. 2.

A Bayesian estimator [36] tries to achieve an estimate $\hat{f}$ of f - which is assumed to be a random process - by having some prior information about the signal to be estimated, summarized in $p_F(f)$, the a-priori pdf of f. Different Bayesian estimators can be defined according to the choice of the Bayesian "risk", i.e., the function of the estimation error $\varepsilon = f - \hat{f}$ we would like to minimize.

The minimum mean square error (MMSE) estimator minimizes the quantity $E[\varepsilon^2] = E[(f-\hat{f})^2]$. It is well-known [36] that the solution is given by

$$\hat{f}^{\text{MMSE}} = E_{F|G}[f|g] \tag{16}$$

which is the expectation of the noise-free signal conditional to the noisy observation. By exploiting the Bayes rule and the

additive signal-dependent model $g = f + v$, we obtain

$$\begin{aligned}\hat{f}^{\text{MMSE}} &= \int f p_{F|G}(f|g) df \\ &= \int f \frac{p_{G|F}(g|f) p_F(f)}{p_G(g)} df \\ &= \frac{\int f p_V(g-f) p_F(f) df}{\int p_V(g-f) p_F(f) df}\end{aligned} \tag{17}$$

The estimate in (17) would require the knowledge of the nonstationary joint pdfs of any orders.

A simpler solution requiring only second order moments is the linear MMSE (LMMSE) estimator, in which the MMSE solution is sought by constraining the estimator to be a linear combination of the observed variables. The LMMSE estimator is given by

$$\hat{f}^{\text{LMMSE}} = E[f] + C_{fg} C_{gg}^{-1} (g - E[g]), \tag{18}$$

in which C_{fg} is the covariance matrix between f and g and C_{gg} is the autocovariance matrix of g. Prior knowledge is now embedded in the second order statistics of the noise-free and noisy signals, which can be derived by exploiting the additive model.

The maximum a-posteriori probability (MAP) estimator minimizes the quantity $E[C(\varepsilon)]$, where $C(\varepsilon) = 1$ for $|\varepsilon| > \delta$ and $C(\varepsilon) = 0$ elsewhere. The solution, when δ is small, is given by

$$\hat{f}^{\text{MAP}} = \arg\max_f p_{F|G}[f|g] \tag{19}$$

Again, by exploiting the Bayes rule and the additive model, we have

$$\begin{aligned}\hat{f}^{\text{MAP}} &= \arg\max_f \; p_{G|F}(g|f) p_F(f) \\ &= \arg\max_f \; p_V(g-f) p_F(f)\end{aligned} \tag{20}$$

or, equivalently,

$$\hat{f}^{\text{MAP}} = \arg\max_f \; [\log p_V(g-f) + \log p_F(f)] \tag{21}$$

Eqs. (17), (18) and (20) reveal that all solutions, besides to the a-priori information on f, require also knowledge of the pdf of the noise component v.

C. Wavelet Transforms

A Bayesian estimation carried out in the spatial domain leads to a solution that adaptively depends on local statistics, i.e., is a space-adaptive estimator. A Bayesian estimation carried out in the multiresolution, or *scale-space*, domain may have the extra value of leading to a scale-space adaptive estimator, that is, an estimator adaptive not only in space but also in scale. Such an extra value is not automatic and requires careful pdf modeling in the transformed domain, otherwise the spatial adaptivity may get lost in favor of the scale adaptivity.

The wavelet analysis provides a multiresolution representation of continuous and discrete-time signals and images [35]. For discrete-time signals, the classical maximally decimated wavelet decomposition is implemented by filtering the input signal with a lowpass filter $H_0(z)$ and a highpass filter $H_1(z)$ and downsampling each output by a factor two. The synthesis of the signal is obtained with a scheme symmetrical to that of the analysis stage, i.e., by upsampling the coefficients of the decomposition and by lowpass and highpass filtering. Analysis and synthesis filters are designed in order to obtain the perfect reconstruction of the signal and by using different constraints (e.g., orthogonal or biorthogonal decomposition, linear phase filters). Applying the same decomposition to the lowpass channel output yields a two-level wavelet transform: such a scheme can be iterated in a dyadic fashion to generate a multilevel decomposition. The analysis and synthesis stages of a two-level decomposition are depicted in Fig. 3-(a).

In several image processing applications, e.g., compression, the DWT is particularly appealing since it compacts energy in few coefficients. However, for most of the tasks concerning images, the use of an undecimated discrete wavelet transform (UDWT) is more appropriate thanks to the shift-invariance property. UDWT is also referred to as *stationary* WT (SWT) [37], [38], as opposite to Mallat's octave (dyadic) wavelet decomposition DWT [35], which is maximally, or *critically*, decimated. The rationale for working in the UDWT domain is that in DWT, when coefficients are changed, e.g., thresholded or shrunk, the *constructive* aliasing terms between two adjacent subbands are no longer canceled during the synthesis stage, thereby resulting in the onset of structured artifacts [39].

As to the construction of the UDWT, it can be shown that if we omit the downsamplers from the analysis stage and the upsamplers from the synthesis stage, then the perfect reconstruction property can still be achieved. The relative scheme for a two-level decomposition is depicted in Fig. 3-(b). In the block diagram, by applying the *noble identities* [40], the downsamplers (upsamplers) have been shifted towards the output (input) of the analysis (synthesis) stage. Eliminating these elements yields the UDWT. As a consequence, the coefficients in the transform domain can be obtained by filtering the original signal by means of the following *equivalent* transfer functions:

$$\begin{aligned}H_{eq,l}^{j}(z) &= \prod_{m=0}^{j-1} H_0(z^{2^m}), \\ H_{eq,h}^{j}(z) &= \left[\prod_{m=0}^{j-2} H_0(z^{2^m})\right] \cdot H_1(z^{2^{j-1}})\end{aligned} \tag{22}$$

where the subscripts l and h refer to the *approximation* (lowpass) and *detail* or *wavelet* (bandpass and highpass) signals, whereas j denotes the level of the decomposition. An example of the equivalent filters frequency responses, relative to a four-level decomposition, is shown in Fig. 4.

Let $A_x^j(n)$ and $W_x^j(n)$ denote the approximation and wavelet coefficients, respectively, of the signal x at the jth level of the decomposition, whereas n is the spatial index. Since the wavelet transform is linear, from equation (14) we have

$$A_g^j(n) = A_f^j(n) + A_v^j(n) \tag{23}$$

$$W_g^j(n) = W_f^j(n) + W_v^j(n) \tag{24}$$

Usually, only the wavelet coefficients (24) are processed for despeckling; the baseband approximation is left unchanged.

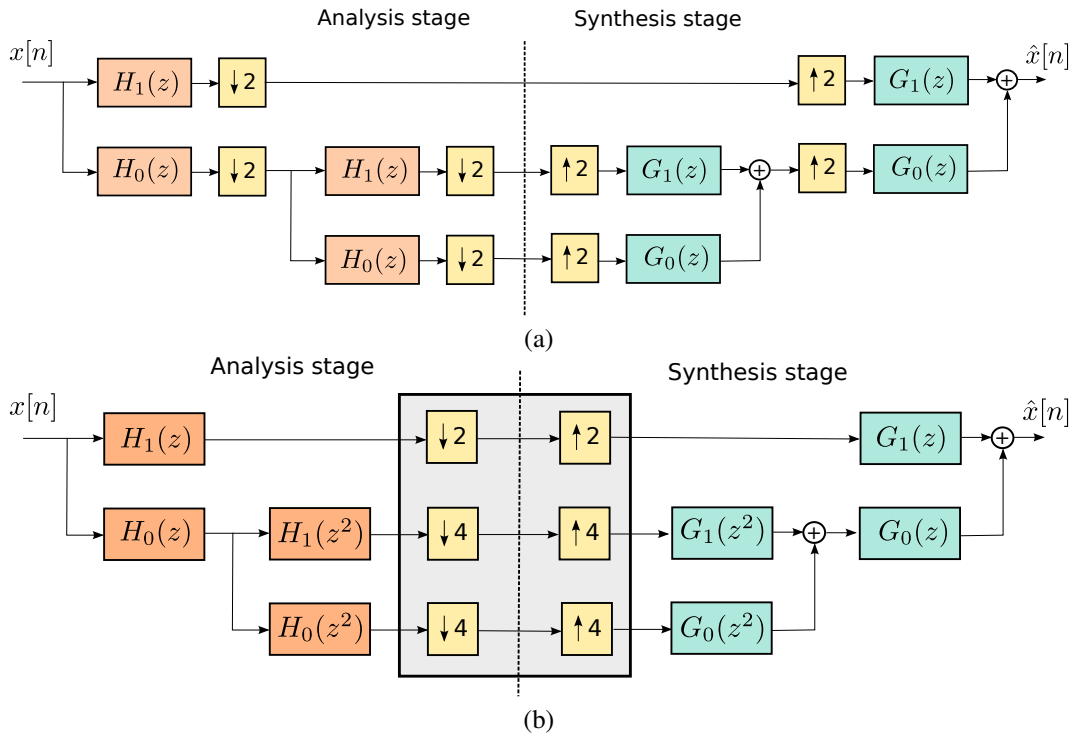

Fig. 3. Two-level nonredundant wavelet decomposition / reconstruction (a) and the equivalent scheme obtained applying the noble identities (b). The undecimated wavelet transform is obtained by eliminating the downsamplers and upsamplers contained in the shaded box.

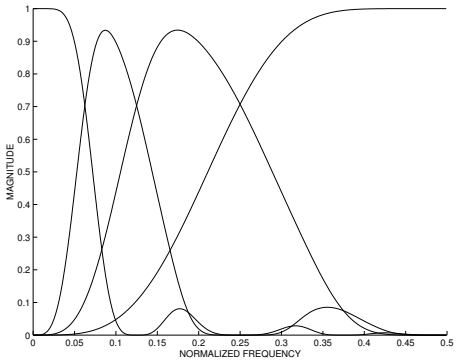

Fig. 4. Equivalent filters frequency responses obtained from 8-tap Daubechies orthogonal wavelets [34].

The wavelet transform is usually implemented for images by using separable filtering along the columns and the rows of the image. The effect of this processing is the extraction, in each subband, of a rectangular region of the frequency plane which corresponds, in the spatial domain, to the extraction of horizontal and vertical details with different degrees of resolution. The frequency plane splitting relative to a single level decomposition is given in Fig. 5-(a). However, extracting directional information has been demonstrated to be useful in several image processing tasks.

Recently, multiresolution transforms embedding directional information, such as contourlets [41], curvelets [42], [43], and many others, have been successfully applied to denoising in general and despeckling in particular. The nonsubsampled contourlet transform is a combination of a nonsubsampled Laplacian pyramid (NLP) decomposition and of nonsubsampled directional filter banks (NDFB). The relative frequency splitting is depicted in Fig. 5-(b). As in the case of the UDWT, also the coefficients of the nonsubsampled contourlet transform can be achieved by means of linear time-invariant (LTI) systems directly applied to the input, which allows statistical parameters to be easily computed. Using directional information is effective in terms of despeckling performance [44], even though a higher computational cost must be paid due to the need of a nonseparable implementation.

By assuming that the transform is linear, the additive models in (14) and (15) can be easily generalized to the transformed domain. Specifically, for the formulation given in (14), if W_x denotes the transform operator applied to the signal x, we have

$$W_g = W_f + W_v, \tag{25}$$

In an analogous way, by applying both the homomorphic filtering concept and the linear transform, the observation model in (15) becomes

$$W_{g'} = W_{f'} + W_{u'}. \tag{26}$$

The Bayesian estimator explicitly derived for the additive model in (14), can also be applied to the additive models defined in (15), (25), and (26) by simply changing the type of variables and prior knowledge, that is: 1) the prior pdf of the signal of interest (related to the reflectivity) and represented by f, f', W_f and $W_{f'}$ in equations (14), (15), (25), and (26), in that order; 2) the pdf of the additive noise component, represented by v, u', W_v and $W_{u'}$, in the same equations.

D. PDF modeling

Bayesian estimation relies on an accurate probabilistic modeling of the signals under concern. However, the choice of pdfs

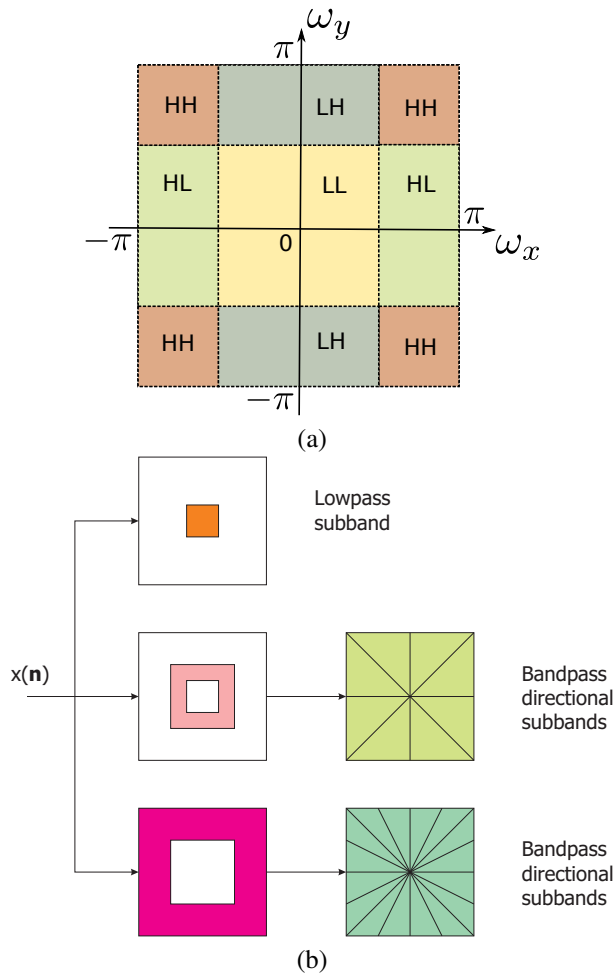

Fig. 5. Frequency splitting from a single-level separable DWT (a), obtained by lowpass (L) and highpass (H) filtering along the rows and the columns (LL, HL, LH, and HH denote all possible combination); in (b), the splitting obtained from the nonsubsampled Laplacian pyramid decomposition (on the left) and the nonsubsampled directional filter banks (on the right) composing the contourlet transform.

suitable for modeling the data of interest is not a simple task. In Section II, we have described some of the most used pdfs for the speckle and reflectivity processes. While the former derive from the image formation mechanism and may be considered as valid in most of the images where the fully developed speckle model holds, the latter highly depend on the imaged scene. We highlight again that different types of landscapes and land covers induce different distributions on the reflectivity signal. Models of the underlying land cover may help to derive a pdf of the imaged signal, but this knowledge may not be available for despeckling or may be insufficient. As to the modeling of signals in the homomorphic domain, an exact derivation of the log-intensity and of the log-amplitude of the fading variable is available [33], whereas the characterization of the backscattering coefficient still remains crucial.

The modeling of the involved variables may be simpler and more robust if one works in a multiresolution, or *scale-space*, domain, instead than in the spatial domain. In fact, it is well-known that the pdf of wavelet coefficients can be approximated by several unimodal distributions - as noticed by Mallat in his seminal paper [35], where a generalized Gaussian was used - that can be described by a small number of parameters. They can be adaptively estimated from the coefficients of the observed image, independently of the distribution of the image that is transformed.

Validating a hypothetical pdf model is, in general, quite hard. In some works, wavelet coefficients pdfs are validated "globally" from the observation of the histogram of the amplitude of the coefficients in a whole subband. However, since the signal is nonstationary, spatially adaptive methods should be used instead. A single observation, or realization, of the scene is usually available; thus, one may only conjecture that wavelet coefficients "locally" follow a given distribution (only few samples are available to perform the validation of the local model) whose parameters locally vary. A way to check the validity of the pdf model is experimentally observing the performances of despeckling filters on either true SAR or synthetically speckled images. As a general rule of thumb, the higher the number of parameters, or degrees of freedom, of the pdf, the better its ability to model the true wavelet coefficients pdf within a whole subband, but the lower their estimation accuracy from the few samples available in a local window within a subband and the higher the complexity of the resulting estimator. Therefore, the use of reasonably simple distributions may be expected to yield better results than more complex ones, that is, *overfitting* is not rewarding.

Another fact that should be considered when a pdf model is chosen is the computational cost. Some combinations of estimation criterion and pdf model yield a Bayesian estimator that can be achieved only numerically [45]. This fact may prevent from using the filter when huge amounts of data need to be processed. In this case, a closed form solution may be preferred, even though a possible loss of performances may be experienced.

IV. A Review of Despeckling Methods

A multitude of despeckling filters can be obtained by combining the different domains of estimation (spatial, homomorphic, wavelet, homomorphic-wavelet), the estimation criteria, e.g., MMSE, LMMSE, minimum mean absolute error (MMAE), MAP or non-Bayesian, and the pdf models. A non-exhaustive review and classification of methods is attempted in the following of this section.

A. Bayesian methods in spatial domain

Early works on despeckling were deployed in the spatial domain and were obtained by making assumptions on the statistical properties of reflectivity and speckle, e.g., pdf and autocorrelation function.

Lee Filter– The *local-statistics* filter, introduced by Jong-Sen Lee in 1980, is reportedly the first model-based despeckling filter. The original paper [21] contained solutions for both additive signal-independent noise and speckle noise. The latter solution was thoroughly developed in [46] and reviewed in [47] together with the sigma filter. An LMMSE solution was derived by linearizing the multiplicative noise model around the mean of the noisy signal. In this way, the author devised

an approximate but effective solution which is identical to the exact solution, apart from the term $(1+\sigma_u^2)^{-1}$, in which σ_u^2 is the variance of the multiplicative noise u. The contribution of this term can be practically neglected for *multi-look* images, in which $\sigma_u^2 \ll 1$ [19], [48].

Lee Refined Filter– This filter [49] was designed to overcome the drawback of edge boundaries that are left noisy by Lee filter. To improve filtering, once an edge is detected in a 7×7 sliding window, the algorithm uses the local gradient to estimate its orientation. Eight edge-directed non-square windows are allowed. The estimation of the local mean and of the local variance are performed within the local window that better fits the edge orientation. If no edge is detected, the estimates are computed on the whole 7×7 window. Filtering results are quite impressive, particularly on edges and high contrast areas. Some artifacts may occur when the filter processes textured areas that result to be overly segmented. Another limitation is that the filter works with a window of fixed size 7×7: textures characterized by a high spatial variation and thin linear features may be altered. An ERS-2 image of Florence is shown in Fig. 6-(a); processing of refined Lee filtering in Fig. 6-(b).

Frost Filter– In Frost filter [50], starting from a model of the coherent imaging system, a parametric approximation of the autocorrelation function of reflectivity is derived from local statistics. Such a function is used to devise an LMMSE solution for the noise-free reflectivity itself. The filtered value is a linear combination of pixel values within the local window with a Gaussian weighting function that depends on the local coefficient of variation of the noisy image g, namely C_g, defined as the ratio of local standard deviation to local mean. Despite its large popularity in the image processing community, Frost filter had no developments over time, either by the authors or by others, apart from the heterogeneity adjustment common to all spatial Bayesian filters [51], which will be reviewed at the end of this subsection.

Kuan Filters– Kuan's filter [52] exactly implements the LMMSE solution (18) starting from a signal model that features nonstationary mean, nonstationary variance and thus a diagonal covariance matrix in (18). The resulting LMMSE solution is referred to as local LMMSE (LLMMSE) to indicate that it contains only local first order statistics, mean and variance, that are easily calculated in a sliding window. Accordingly, the optimum estimate of reflectivity, $\hat{f}$, is given as a combination of the unfiltered noisy pixel value g and of its local average $\bar{g}$, approximating the local mean, with weights nonnegative and summing to one. The center pixel is more or less weighted depending on its local signal to noise ratio (SNR). Besides despeckling, also restoration for the effects of the imaging system can be carried out [53]. The price is a considerable increment in the computational complexity of the procedure.

MAP Filters– The prototype of MAP filters in spatial domain is the Γ-MAP filter, introduced in [54] and thoroughly analyzed in [55]. It assumes that both the radar reflectivity and the speckle noise follow a Gamma distribution and solves the MAP equation (21) accordingly. It is designed to smooth out noise while retaining edges or shape features in the image. Different filter sizes greatly affect the quality of processed images. If the filter is too small, the noise filtering algorithm is not effective. If the filter is too large, subtle details of the image will be lost in the filtering process. A 7×7 filter usually gives the best tradeoff.

A refined version of the Γ-MAP filter that features an improved geometrical adaptivity, analogously to Lee refined filter, was proposed in [56]. The visual result appears in Fig. 6-(c). This achievement marks the beginning of a certain performance saturation in spatial despeckling methods, although highly sophisticated Bayesian methods in space domain, featuring MAP estimation associated to, e.g., Gauss-Markov and Gibbs random fields for prior modeling have been introduced later [57] and are still used [58].

Despeckling Filters and SAR Heterogeneity– The filters described in this subsection can be adjusted to the heterogeneity of SAR images, as suggested in [51]. The rationale is that in true SAR images at least three statistical classes can be recognized: homogeneous, textured, and strong, or *persistent*, scatterer. The first class is characterized by a spatially constant reflectivity and in this case the best estimator is a plain average of intensity pixel values in a neighborhood. Pixel belonging to the third class should be detected and left unprocessed, as they are intrinsically noise-free and are used for calibration, registration, etc. The intermediate class may be processed through the desired filter, e.g., Lee, Frost and Kuan filters. The resulting filters are known in the literature as *enhanced* Lee, Frost and Kuan filters [51]. The Γ-MAP filters was originally defined in *enhanced* version [54]. The three classes are found by thresholding C_g. The two thresholds, namely C_{min} and C_{max} are empirically set equal to σ_u, the standard deviation of speckle, and $\sqrt{3}\sigma_u$ [51].

B. Bayesian methods in transform domain

Apart from a few methods that employ multiresolution concepts without a formal multiresolution analysis, like Meer's filter and especially the filter based on the Laplacian pyramid, all filters reviewed in this subsection exploit the discrete wavelet transform, either decimated or not.

Meer's Filter– Meer's filter [60] considers a local neighborhood constituted by a set of three concentric sliding windows, 7×7, 5×5 and 3×3. A homogeneity index is given by C_g, computed over each of the windows. The spatial average on the largest window satisfying a homogeneity criterion, defined by thresholding its C_g, is given as output. If such a window does not exist, Kuan's LLMMSE estimate on the innermost 3×3 window is assigned to the center pixel. This filter is effective in preserving point targets, linear features and edges, thanks to its capability to shrink its window size. Performances on point targets and linear features are slightly better than those of Lee's refined filter which, however, is superior on linear edges.

RLP Filter– The rational Laplacian pyramid (RLP) filter [59] is an evolution for speckle filtering of the denoising method

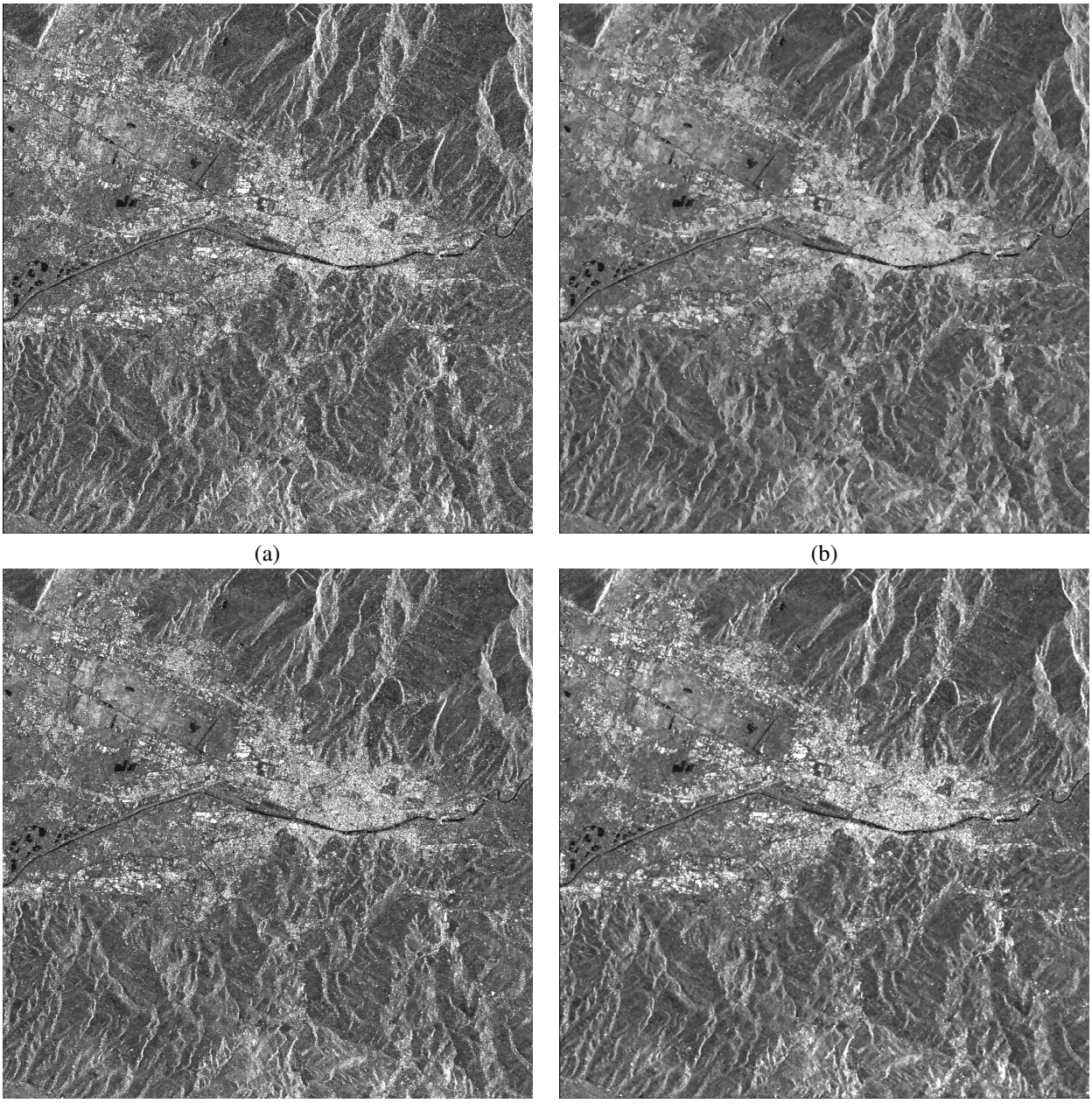

Fig. 6. Examples of the application of Bayesian estimators in the UDWT domain: (a) original 5-look ERS-2 image and filtered versions obtained with (b) Lee refined filter [49]; (c) refined Γ-MAP filter [56]; (d) Rational Laplacian Pyramid filter [59].

based on the enhanced Laplacian pyramid [61]. The latter is commonly used for spatially scalable layered video coding as well as for lossless and near lossless compression of still images by exploiting quantization noise feedback [62], [63].

RLP differs from LP because its passband layers are obtained by taking the ratio pixel by pixel between one level of the Gaussian pyramid and the interpolated version of the lower resolution upper level. While the baseband icon, corresponding to the top of the Gaussian pyramid, may be left unprocessed because of its high SNR obtained through cascaded lowpass filtering and decimation stages, analogously to multi-looking, the bandpass levels of RLP are processed by means of Kuan's filter [52]. The despeckled image is synthesized from the denoised RLP. This multiscale LMMSE filter outperforms its spatial counterpart thanks to multiresolution processing. The result of RLP filtering can be watched in Fig. 6-(d).

Homomorphic Filtering in Wavelet Domain– Filtering in the wavelet-homomorphic domain (see Fig. 2-(d)) has been extensively used during the last twenty years and potentially superior performances over conventional spatial filters have been recognized [64], [65]. In fact, each wavelet subband is associated to a speckle contribution that may be exactly measured [66] and filtered out. Thus, spatially adaptive filtering become also scale-adaptive.

Classical hard- and soft-thresholding methods [67] were applied in [68]. Thresholding based on nonlinear functions

(sigmoid functions), adapted for each subband, has been used in [69]. In [70], MMSE estimation has been used associated to a combination of generalized Gaussian (GG) / Gaussian pdfs for the reflectivity and for the noise components, respectively. In [71], MMSE estimation have been used after modeling wavelet coefficients by means of Gaussian mixtures and Markov random fields to characterize their spatial and inter-scale dependency. In [72], the MAP criterion has been used associated to α-stable distributions for the prior of the signal and to a log-normal pdf for the noise. In [73], MAP estimation is applied based on normal inverse Gaussian distributions. In [74], MMAE estimation has been used associated to a Cauchy prior for the reflectivity signal and to a Gaussian pdf for the noise; the previous method has been extended to the MAP criterion in [75]. In [76], MAP estimation is used associated to a heavy-tailed Rayleigh prior for the signal and to Gamma or Nagakami models (for images in intensity or amplitude format, respectively) for the noise.

Non-Homomorphic Filtering in Wavelet Domain– Non-homomorphic wavelet-domain despeckling (see Fig. 2-(c)) has been considered less frequently in the literature. Even though the absence of the bias due to the nonlinear mapping of the logarithm is an advantage, the estimation of the parameters of the signal and noise pdfs becomes more complex. In fact, in the equivalent additive-noise model for the non-homomorphic case, the noise term is signal-dependent and, therefore, its parameters are much more difficult to be estimated.

In the seminal paper by Foucher *et al.* [77], undecimated wavelet was firstly used for despeckling. Estimation is based on the MAP criterion and the Pearson system of distributions. In [78], the LMMSE estimator, optimal under the Gaussianity assumption, has been presented. In [79], the LMMSE estimator with mixtures of Gaussian pdfs is enforced by the use of the ratio edge detector [80] to improve despeckling of contours. In [81], MAP estimation is used along with the assumption of normal inverse Gaussian distributions for the wavelet coefficients. MAP estimation associated to locally-varying generalized Gaussian (GG) distributions has been used in [82]. In [83] a segmentation-based MAP despeckling with GG priors is achieved. The method in [82] has been extended to the domain of the nonsubsampled contourlet transform (NSCT) in [44]. Another method in the contourlet domain has been proposed in [84]. MAP and MMSE estimators associated to Laplacian and Gaussian PDFs for the signal and noise components have been proposed in [85]. Generalized Γ and Gaussian distributions have been used for MAP despeckling in [86], [87]. An interesting example of despeckling not pertaining SAR but ultrasound images and based on statistical classification of signal/noise wavelet coefficients is presented in [88]. Also non-Bayesian methods based on the classification of signal and noise wavelet coefficients have been proposed in [89], [90].

C. Non-Bayesian approaches

A number of despeckling filters published over the last thirty years do not follow a Bayesian approach. In the following, the most popular approaches and related methods are summarized.

Order Statistics and Morphological Filters– Starting with median filter, order-statistics filters encountered a certain popularity for despeckling, thanks to their peculiar features of edge preservation. A conditional version of median filter [91], replaces the central pixel value of the local sliding window with the sample median if and only if the former is recognized as an outlier, i.e., an extremal value within the window. An adaptive version of the weighted median filter was specifically proposed for despeckling [92]. It is substantially a center-weighted median filter, in which the weight is adaptively calculated from local statistics, in order to preserve edges, retain textures and smooth the noisy background.

Geometric filter (GF) [93] is a powerful tool for edge-preserving smoothing of noise and especially of speckle, the purpose it was designed for. GF iteratively erases noise samples regarded as geometric artifacts of the 3-D shape defined by the 2-D gray-level function. GF is a nonlinear local operator that exploits a morphologic approach to smooth noise one image line at a time using a complementary hull algorithm, whose iterations converge towards *roots*, i.e., steady patterns invariant to further iterations, in which spatial details thinner than a critical size are completely suppressed. Thicker objects are just slightly smoothed and therefore fairly preserved as filtering is iterated. A decimated version of GF [94], suitable for spatially correlated noise, including speckle, consists of applying GF to fhe four polyphase components, in which the original image is preliminarily decomposed, and of re-interleaving the filtered components to yield the denoised image.

None of the methods reported above explicitly accounts for the speckle noise model. However, their computational speed together with the capability of preserving abrupt discontinuities of level was found to be of interest in computer vision and object recognition applications. Nowadays these methods are less and less frequently used, though they might be valuable for high-resolution images of man-made environments, in which persistent scatterers and not fully developed speckle are frequently encountered.

Anisotropic Diffusion– Anisotropic diffusion [95] is a technique, extremely popular in the image processing community, that aims at reducing image noise without removing significant parts of the image content, typically edges, lines or other details that are important for the interpretation of the image. The derivation speckle reducing anisotropic diffusion (SRAD) is tailored to coherent images [96]. SRAD is the edge-sensitive diffusion for speckled images, in the same way that conventional anisotropic diffusion is the edge-sensitive diffusion for images corrupted with additive noise. Just as the Lee and Frost filters utilize the coefficient of variation in adaptive filtering, SRAD exploits the instantaneous coefficient of variation, which is shown to be a function of the local gradient magnitude, and Laplacian operators. SRAD overcomes traditional speckle removal filters in terms of mean preservation, variance reduction, and edge localization. However, the unrealistic smoothness introduced after iterated processing makes SRAD unsurpassed for cartoon-like images, i.e., made up by textureless geometric patches, but may be unsuitable for

real SAR images, because fine details and textures that may be useful for analysis are destroyed. A notable application of SRAD is for coastline detection in SAR images [97].

Simulated Annealing Despeckling– Simulated Annealing (SA) was originally used for SAR image despeckling and segmentation by White [98]. SA is a stochastic optimization method used for finding the global maximum of an a-posteriori multivariate distribution, or equivalently the global minimum of a multidimensional energy function, which is often made difficult by local maxima (minima), which can easily trap the optimization algorithm. SA is iterative by nature, where a new configuration for iteration is found from the previous configuration by applying a generation mechanism and accepting the new configuration using an acceptance criterion based on the energy divergence. The *temperature* variable controls the optimization, and it is decreased throughout the optimization process. For the first iterations, when it is high, there is a high probability of accepting configurations resulting in an increase in the energy, thus making SA able to get out of local minima. As the temperature is gradually decreased, the probability of accepting configurations resulting in increasing energies is reduced, so that at the end of the minimization no increases are accepted, and the global minimum configuration is ideally reached. Despite its potentiality, the unlikely cartoon-like smoothness produced by SA was noticed in [99]. After that, SA was used only in conjunction with complex multivariate pdf models, like in polarimetric SAR [100].

Sigma Filter– A conceptually simple noise smoothing algorithm is the sigma filter originally developed for additive signal-independent noise [101] and promptly extended to speckle removal [102] also in a comparison with local-statistics filtering [47]. This filter is motivated by the sigma probability of the Gaussian distribution, and it smooths the image noise by averaging only those neighborhood pixels which have the intensities within a fixed sigma range of the center pixel. Consequently, image edges are preserved, and subtle details and thin lines, such as roads, are retained.

An enhanced version of Lee's sigma filter [103] is derived and proposed for unbiased filtering of images affected by multiplicative noise with speckle statistics. Instead of the plain point value, a more accurate start value is first produced, and then fed to the procedure of conditional average. A robust estimate of the nonstationary mean is defined according to a decision rule. The start value is provided by a nonlinear decision rule, aimed at rejecting noisy samples, that is performed on the averages computed within four isotropically balanced pixel sets able to capture step edges and thin lines. The level range of pixels to be averaged, adaptively defined as the product of the space-variant mean estimate by the constant noise variance, is also forced to account for the imbalance of the noise distribution, for unbiased processing.

Eventually, in [104] the bias problem is solved by redefining the sigma range based on the speckle pdf. To mitigate the problems of blurring and depressing strong reflective scatterers, a target signature preservation technique is developed. In addition, the LLMMSE estimator for adaptive speckle reduction [21], [52] is incorporated.

Bilateral Filtering– The bilateral filter (BF), originally introduced in [105] for gray scale images, has been recently extended to despeckling in [106]. The rationale of BF is that each pixel value within a sliding window is weighted both for the distance to the center, as in Frost filter, and for the difference to the value of the center, as in sigma filter. In an adaptive version of BF suitable for despeckling [107], the spatial weighting is a Gaussian function, whose span depends on the local coefficient of variation, analogously to the enhanced Frost filter. A rule borrowed from [108] defines the weights as the gray level difference between the central pixel and each neighboring pixel, as the probability of two values in a speckled image that exhibit the same reflectivity value. The adaptive method in [107] exploits an order statistic filter, like [91], to reject outliers that often occur. Despite its elegance and relatively low computational cost, in the presence of strong noise, like for single-look images, speckle-oriented BF suffers from limitations given by the finite size spatial function, same as all local spatial filters. A way to overcome such a drawback is adopting a nonlocal filtering approach.

Nonlocal Filtering– Among the despeckling methods that cannot be included in the classical Bayesian framework, nonlocal (NL) filtering is surely one of the most interesting and promising solutions [108], [109]. NL filtering is a generalization of the concept of data-driven weighted averaging, in which each pixel is weighted according to its similarity with the reference pixel, as in the pioneering sigma filter. The NL mean filter [110] extends the above method, by defining the weights as a function of the Euclidean distance between a local patch centered at the reference pixel and a similar patch centered at a given neighboring pixel. The block-matching 3-D filter (BM3D) [111] combines the advantages of the NL principle and of the wavelet representation: 3-D groups of pixels are formed by collecting blocks of pixels drawn from different image locations and chosen according to their similarity with a reference block, and Wiener filtering is applied to the wavelet coefficients of such 3-D groups.

In [108], NL filtering has been applied to despeckling by substituting the Euclidean distance used in the NL mean filter with a probabilistic measure that takes into account the pdf of SAR data, and by proposing an iterative procedure for refining the weights. Following a similar approach, an improved similarity measure has been recently proposed in [112]. Other approaches consider a Bayesian NL framework [113], which has been applied to the despeckling of both ultrasound images [114] and SAR images [115]. The NL principle has been successfully applied also to despeckling in the wavelet domain [109], [116]. Namely, in [109] the authors extend the BM3D filter by redefining the similarity measure among block of pixels according to [108], and employing the LLMMSE principle [78] in the estimation step.

Total Variation Regularization– Another popular denoising approach is based on total variation (TV) regularization [117]. In such a method, denoising is achieved through the minimization of a suitable cost function, combining a data

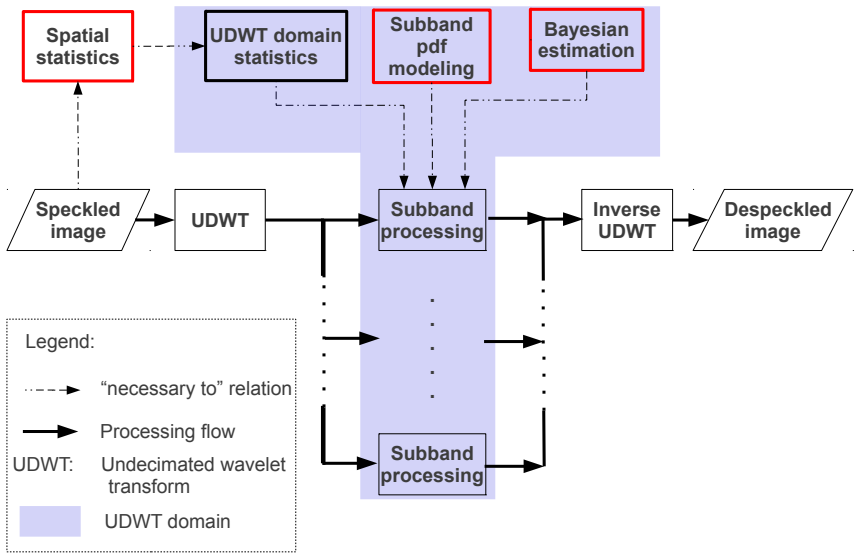

Fig. 7. Flowchart of Bayesian filtering in the undecimated wavelet domain.

fidelity term with a prior that enforces smoothness while preserving edges. Several solutions exist to apply TV methods in the case of multiplicative noise [118]–[124]. These solutions differ according to the domain in which the optimization is performed, which can be either the intensity or the logarithm of the intensity, and the definition of the data fidelity term. In [119], the authors define the optimization problem in the original intensity domain and apply a data fidelity term based on a maximum a posteriori approach, assuming a Gamma distributed speckle and a Gibbs prior. Due to the difficulty of defining strictly convex TV problems in the original intensity domain, several authors have considered the logarithmic domain instead. When applying TV regularization in the logarithmic domain, convex TV problems can be obtained by applying different data fidelity terms, including the L_2 norm [120], MAP based on Gamma distributed speckle [120], [124], a combination of the previous terms [121], the generalized Kullback-Leibler divergence [123], the L_1 norm on curvelet coefficients [122]. It is worth noting that all the above methods have been mainly validated on simulated data. The literature regarding the application of such methods to actual SAR images is quite scarce [125]–[127], and there is a general lack of comparisons with Bayesian and NL despeckling methods.

Despeckling based on Compressed Sensing– A new signal representation model has recently become very popular and has attracted the attention of researchers working in the field of restoration of images affected by additive noise as well as in several other areas. In fact, natural images satisfy a *sparse* model, that is, they can be seen as the linear combination of few elements of a *dictionary* or *atoms*. Sparse models are at the basis of *compressed sensing* [128], which is the representation of signals with a number of samples at a sub-Nyquist rate. In mathematical terms, the observed image is modeled as $y = Ax + w$, where A is the dictionary, x is a sparse vector, such that $\|x\|_0 \leq K$, with $K \ll M$, with M the dimension of x, and w is a noise term that does not satisfy a sparse model. In this context, denoising translates into finding the sparsest vectors with the constraint $\|y - Ax\|_2^2 < \epsilon$, where ϵ accounts for the noise variance. The problem is NP-hard, but it can be relaxed into a convex optimization one by substituting the pseudo-norm $\|\cdot\|_0$ with $\|\cdot\|_1$. Recently, some despeckling methods based on the compressed sensing paradigm and sparse representations have appeared [129]–[131].

V. Multiresolution Bayesian Filtering

In this section, we review some methods recently proposed for despeckling in the undecimated wavelet domain that use a multiresolution analysis. The methods refer to the additive model in (26), that is, they do not exploit the homomorphic transform, which may introduce bias in the estimation of the despeckled image.

Fig. 7 outlines the flowchart of Bayesian despeckling in UDWT domain. As it appears, the majority of processing is carried out in the transform domain. Statistics in the transform domain are directly calculated from the spatial statistics of the image by exploiting the equivalent filters (4), as firstly proposed by Foucher *et al.* [77].

A. LMMSE filter

In the case of zero-mean Gaussian pdf modeling for the quantities W_f and W_v, the MMSE and MAP Bayesian estimators are identical. The expression of the filter has a simple and closed analytical form that depends only on the space-varying variance of the wavelet coefficients [78], that is

$$\hat{W}_f^{LMMSE} = W_g \cdot \frac{\sigma^2_{W_f}}{\sigma^2_{W_f} + \sigma^2_{W_v}} = W_g \cdot (1 + \mathrm{SNR}^{-1})^{-1}. \quad (27)$$

Thus, LMMSE estimation corresponds to a *shrinkage* of the noisy coefficient by a factor inversely related to its SNR. Unfortunately, the wavelet coefficients of noise–free reflectivity do not respect the Gaussian assumption, especially in the lowest levels of the wavelet decomposition, so that its performance are inferior to more complex Bayesian estimators. In Fig. 10-(a) a single-look COSMO-SkyMed image is shown. In Fig. 10-(b) the despeckled image obtained by applying the LMMSE estimator is presented.

B. MAP filters

In this section, we present two different filters that use the MAP estimation criterion but different models for the pdfs of the wavelet coefficients relative to the original reflectivity and to the additive signal–dependent noise.

Equation (21) can be rewritten as

$$\hat{W}_f^{\text{MAP}} = \arg\max_{W_f} [\ln p_{W_V|W_F}(W_g - W_f|W_f) + \ln p_{W_F}(W_f)] \quad (28)$$

Since the signal and noise processes are nonstationary, space-varying pdfs must be considered. The pdfs that are considered here can be seen as a trade-off between simplicity (few parameters to be estimated from the observed data) and modeling capability.

MAP–GG filter– In [82], the MAP criterion is combined with a generalized Gaussian (GG) distribution for the wavelet coefficients. Since the birth of the wavelet recursive algorithm by Mallat [35], a GG pdf has been used to model image wavelet coefficients and several other authors use the GG distribution for many image processing tasks involving wavelets. A zero-mean GG pdf depends only on two parameters and is characterized by being symmetric around the mean. Its expression is given by

$$p_X(x) = \left[\frac{\nu \cdot \eta(\nu,\sigma)}{2 \cdot \Gamma(1/\nu)}\right] e^{-[\eta(\nu,\sigma)\cdot|x|]^\nu}, \quad (29)$$

where Γ is the Gamma function, σ is the standard deviation of the distribution, ν is a *shape factor*, and $\eta(\nu,\sigma)$ is given by

$$\eta(\nu,\sigma) = \frac{1}{\sigma}\left[\frac{\Gamma(3/\nu)}{\Gamma(1/\nu)}\right]^{1/2}. \quad (30)$$

The GG distribution is reasonably simple, since the use of only two parameters allows different levels of "peakedness" to be achieved. As particular cases, the GG pdf includes both the Laplacian and the Gaussian pdfs, for $\nu = 1$ and $\nu = 2$, respectively. A plot of GG pdf curves for different values of ν is shown in Fig. 8

Substituting (29) into (28) yields

$$\hat{W}_f^{\text{MAP}} = \arg\max_{W_f}\left[\ln\frac{\eta_{W_f}\nu_{W_f}}{2\Gamma(1/\nu_{W_f})} - \left(\eta_{W_f}|W_f|\right)^{\nu_{W_f}} \ln\frac{\eta_{W_v}\nu_{W_v}}{2\Gamma(1/\nu_{W_v})} - \left(\eta_{W_v}|W_g - W_f|\right)^{\nu_{W_v}}\right] \quad (31)$$

In [82], a method for the estimation of the parameters relative to the GG model, i.e., the standard deviation σ and the shape factor ν of the distributions relative to W_f W_v, is given. The estimation of the parameters is based on the computation of some moments of the observable variables g and W_g. In the implementation of the filters, these moments are substituted by spatial averages. The solution of equation (31) is not known in a closed analytical form and a numerical optimized solution has been proposed in [82].

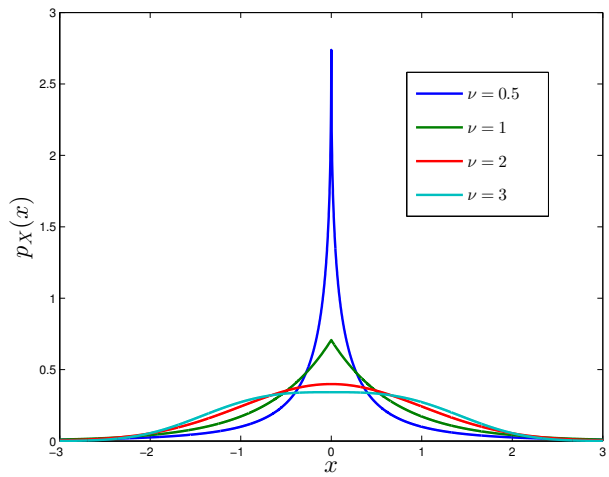

Fig. 8. Zero-mean GG pdfs obtained with unity variance and different νs.

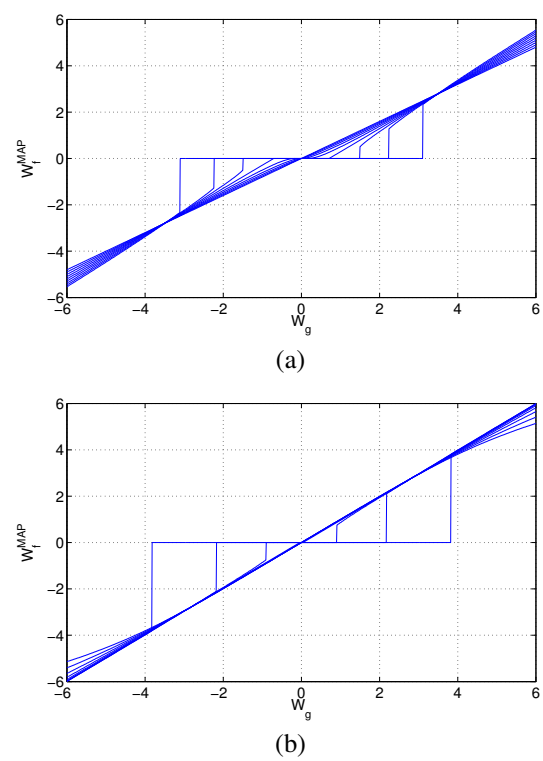

Fig. 9. Mapping of the $\hat{W}_f^{\text{MAP}}$ estimates vs the observed W_g: in (a) $\sigma_{W_f} = 2$, $\sigma_{W_v} = 1$, $\nu_{W_v} = 2$ and ν_{W_f} varies from 0.4 to 2 with step 0.2; in (b) $\nu_{W_v} = 1.2$ (the other parameters are unchanged).

In Fig. 9, a set of curves plotting $\hat{W}_f^{\text{MAP}}$ vs W_g is given for particular values of the parameters of the GG model: in Fig. 9-(a), the curves refer to $\sigma_{W_f} = 2$, $\sigma_{W_v} = 1$, $\nu_{W_v} = 2$ and to ν_{W_f} varying from 0.4 to 2 with step 0.2; in Fig. 9-(b), the

parameter ν_{W_v} has been changed to 1.2 (the other parameters were not modified). Such curves define a remapping of the observed coefficients onto noise-free ones in a similar as done by hard and soft-thresholding schemes proposed commonly used for denoising signals affected by additive signal-independent noise [67], [132]. It is important, however, to point out that for despeckling the wavelet coefficients are modified according to the multiplicative model of speckle and thus adaptively vary according to the locally estimated parameters.

MAP–LG filter– In [85], the empirical distribution of the shape factor of noise–free reflectivity coefficients has been investigated and an interesting behavior was noticed. For the lowest levels of decomposition, the shape factor is usually very close to one, whereas it tends to shift towards two in highest ones. The shape factor of signal–dependent noise coefficients, instead, are mostly concentrated around the value two. These facts suggest directly introducing a combination of Laplacian and Gaussian pdfs into the modeling: this yields some computational advantages with respect to using the more general GG pdf. In fact, by assuming that the wavelet coefficients W_v and W_f follow a zero-mean Gaussian and zero–mean Laplacian distribution, respectively, yields the following closed form estimator [133]:

$$\begin{aligned}\hat{W}_f^{\text{MAP}} &= \arg\max_{W_f} \; p_{W_f|W_g}(W_f|W_g) \\ &= \begin{cases} W_g - \rho, & \text{if } W_g > \rho \\ W_g + \rho, & \text{if } W_g < -\rho \\ 0 & \text{otherwise} \end{cases} \end{aligned} \tag{32}$$

where $\rho = \sqrt{2}\sigma^2_{W_v}/\sigma_{W_f}$. Thus, the estimator is equivalent to a soft-thresholding algorithm with a locally adaptive threshold. Eq. (32) has been originally devised in [134] and used for processing ultrasound images with decimated wavelets.

C. Adjustments for SAR image heterogeneity

In several despeckling methods, different filtering strategies are used according to the texture content of the scene. In [51], [54], the coefficient of variation is used to discriminate among homogeneous, textured and highly heterogeneous (or point target) areas. Pixel belonging to the first two classes are filtered by using simple averaging and Γ-MAP, or another local-statistics filter, whereas no filtering is attempted on point targets. A strongly scattering target, however, is concentrated in space, but after wavelet analysis its response will be somewhat spread because of the finite support of the wavelet function. Thus, also UDWT coefficients around a point target one pixel wide will depend on the target response, unlike what happens in space. In the past, this was perhaps the main objection towards a systematic use of the wavelet transform to analyze SAR images. Starting from [83] a preprocessing step of point targets, and thicker strong scatterers in general, was devised. Targets are detected as upper percentiles of the image histogram, removed from the image and stored. Void pixels are smoothly filled by interpolating their neighbors. Then, wavelet analysis is performed. After synthesis of the despeckled image, point targets are reinserted in their original places.

The leftover two classes, namely homogeneous and textured, can be handled also by multiresolution methods to improve their performance. In [83], UDWT subbands are segmented into texture classes according to an energy index computed in the UDWT domain. Several classes of texture, from textureless onward, can be recognized. The wavelet coefficient of each segment on each subband are supposed to have a unique shape factor of the GG function, while the variance is calculated for each coefficient. Thus, the calculation of the ν is more accurate than in [82], thanks to the more consistent sample size. In [85], the segmentation has been extended to the MAP-LG filter. This time there are no parameters to estimate on segments, as for GG. Thus, a classified approach consists of switching among different estimators, e.g., MAP-LG and LMMSE, depending on the degree of texture of each segment. In Fig. 10-(c) and 10-(d), the results of MAP-GG and MAP-LG estimators, the former with segmentation (GG–MAP–S), the latter with classification (LG–MAP–C), on the image in Fig. 10-(a) are shown.

A segmentation based approach seems also a natural solution to changes in the speckle model occurring as the spatial resolution of single-look products increases. This happens for very high resolution (VHR) new generation SAR systems, especially with Spotlight products. As the size of the elementary resolution cell decreases, the assumption of *distributed scatterers* is less and less verified. In substance, what is homogeneous at 10 m scale may no longer be so at 1 m. So, we expect that VHR SAR images are more textured and contain more persistent scatterers, and less homogeneous regions, than earlier products. A viable solution with segmented processing in UDWT domain is introducing corrective factors for under-smoothing in textured segments, depending on the class of texture energy measured in the UDWT domain, analogously to what proposed in [78].

VI. Non-Local Mean Filtering

The NL mean (NLM) filter proposed by Buades *et al.* in [110] is based on the simple idea of estimating the noise free image as a weighted average of noisy pixels

$$\hat{f}(n) = \frac{\sum_m w(n,m) g(m)}{\sum_m w(n,m)} \tag{33}$$

where the weights $w(n,m)$ take into account the "similarity" between pixels $g(n)$ and $g(m)$. The key idea of the NLM filter is that the weights $w(n,m)$ are based on the Euclidean distance between local patches centered at $g(n)$ and $g(m)$, according to

$$w(n,m) = \exp\left(-\frac{1}{h}\sum_k \alpha_k |g(n+k) - g(m+k)|^2\right) \tag{34}$$

where α_k's define a Gaussian window and h controls the decay of the exponential function.

The NLM filter obtains a very good performance in the presence of additive white Gaussian noise, since the Euclidean distance is a natural similarity measure for this kind of model. However, in the case of SAR images, the weights have to be generalized to the case of multiplicative and non-Gaussian

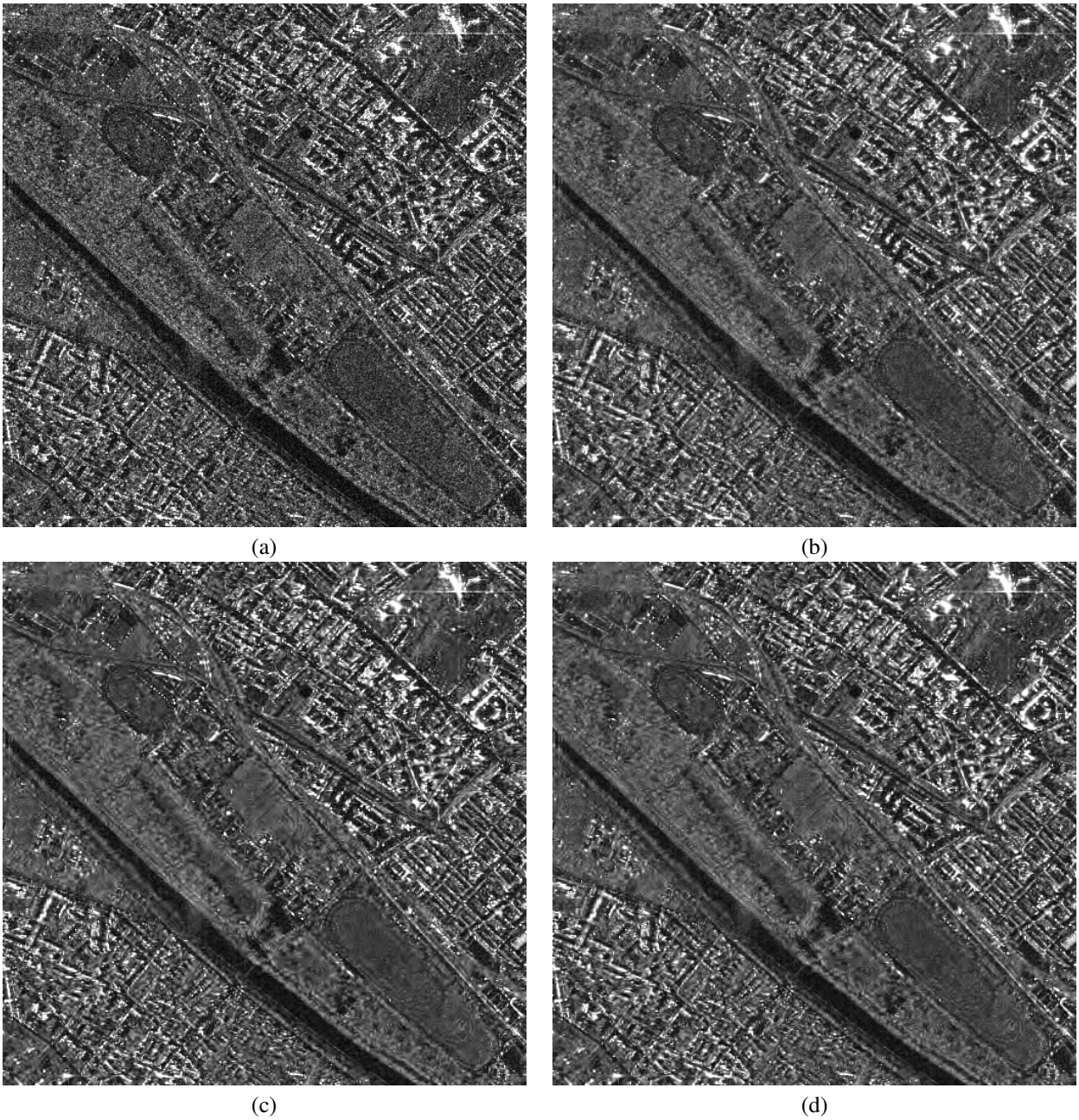

Fig. 10. Examples of the application of Bayesian estimators in the UDWT domain: (a) original COSMO-SkyMed 4-look StripMap image; filtered versions obtained with (b) LMMSE; (c) MAP-GG with segmentation (GG–MAP–S) (d) MAP-LG with classification (LG–MAP–C).

speckle. It is also interesting to combine the effectiveness of the NL principle with the benefits of the sparse representation offered by the wavelet transform. In the following, we will review two SAR despeckling filters based on the NL principle in the spatial [108] and in the wavelet domain [109].

A. Probabilistic Patch-Based Filter

The probabilistic patch-based (PPB) filter, proposed by Deledalle *et al.* in [108], extends the NLM filter to the domain of SAR images by exploiting its connections to the weighted maximum likelihood extimator (WMLE). Namely, under the WMLE principle the noise-free image can be estimated as the value maximizing a weighted likelihood function of the observed data

$$\hat{f}(n) = \arg\max_{f} \sum_{m} w(n,m) \log p(g(m)|f). \qquad (35)$$

In the above equation, the weights $w(n,m)$ can be thought of as a measure indicating to what extent a pixel at position m has the same distribution as the reference pixel at position n.

The definition of the weigths $w(n,m)$ is the key problem of the WMLE approach. In the PPB filter, this problem is solved by expressing the weights as the probability, given the observed image g, that two patches centered at positions n and m can be modeled by the same distribution. By assuming the independence of the pixels of the patches, the weights can be

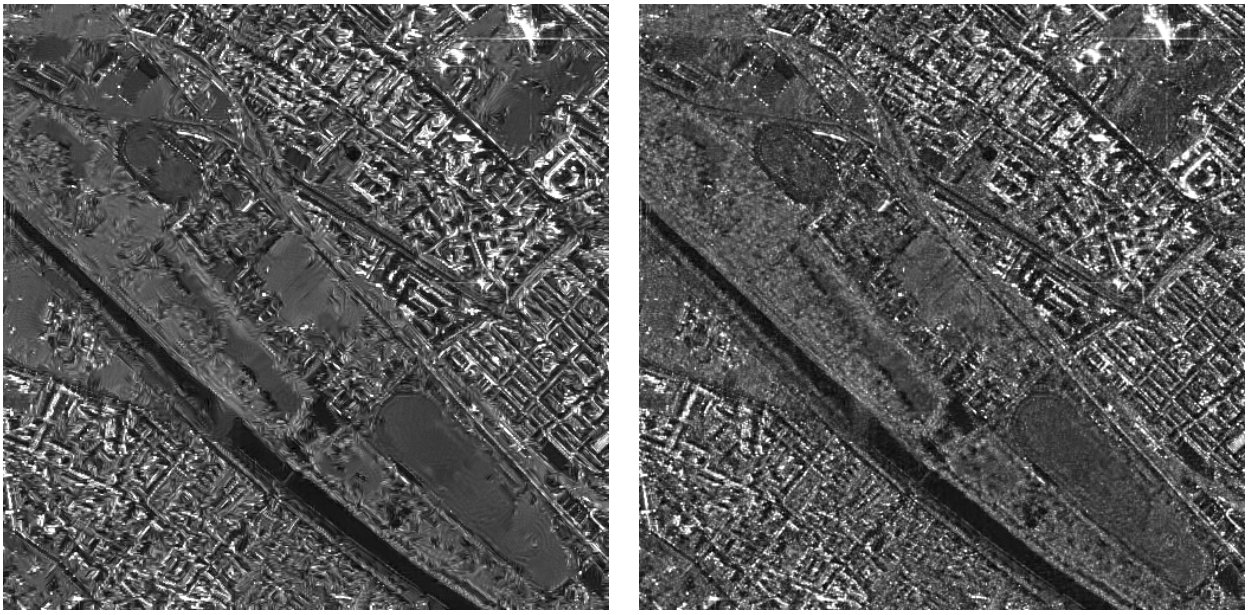

(a) (b)

Fig. 11. Examples of the application of (a) PPB filter and (b) SAR–BM3D filter to the 4-look COSMO-SkyMed image in Fig. 10-(a).

formally expressed as

$$w(n,m) = \prod_k p(f(n+k) = f(m+k)|g(n+k), g(m+k))^{1/h} \tag{36}$$

where k varies over the image patch and h is a decay parameter. According to a Bayesian framework, without knowledge of the prior probabilities $p(f(n+k) = f(m+k))$, the posterior probabilities in equation (36) can be assumed proportional to the likelihood $p(g(n+k), g(m+k)|f(n+k) = f(m+k))$. This permits to adapt the weights of the PPB filter to several image distributions. For the case of SAR images, by assuming that pixel amplitudes $a = \sqrt{g}$ are modeled as independent and identically distributed according to a Nakagami-Rayleigh distribution, the PPB weights can be derived as [108]

$$w(n,m) = \exp\left[-\frac{1}{h}\sum_k \log\left(\frac{a(n+k)}{a(m+k)} + \frac{a(m+k)}{a(n+k)}\right)\right] \tag{37}$$

and the despeckled image can be obtained according to the WMLE as

$$\hat{f}(n) = \frac{\sum_m w(n,m)a^2(m)}{\sum_m w(n,m)}. \tag{38}$$

In [108], the model is further improved by letting the probabilities in (36) depend also on a previous estimate of the noise-free image. This leads to an iterative filtering approach, in which the weights are updated at each iteration according to the previous result of the filter. For the detailed derivation of the iterative PPB filter, the interested reader is referred to [108].

An example of the application of the PPB filter to the COSMO-SkyMed image in Fig. 10-(a) is given in 11-(a). As it appears, PPB filtering overly smooths textures, if any, and tries to achieve a hard segmentation of the scene also in the presence of softly switching classes.

B. SAR Block Matching 3-D Filter

The SAR block matching 3-D (SAR-BM3D) filter, proposed by Parrilli *et al.* in [109], is a SAR-oriented version of the block matching 3-D filter [111], which applies the NL principle in combination with a wavelet representation. The key idea of the BM3D filter is to apply the NL principle for collecting groups of similar image patches, and to compute a wavelet decomposition of the resulting 3-D blocks. The NL grouping of similar patches is expected to form a highly correlated 3-D signal, which will likely have a very sparse representation in the wavelet domain, leading to an effective separation of noise–free and noisy coefficients.

The processing flow of the BM3D filter can be summarized by the following steps: 1) for each reference patch in the observed image, collect the most similar patches according to a Euclidean distance criterion, and form a 3-D group; 2) apply 3-D wavelet transform, denoising of wavelet coefficients, and inverse transform; 3) return all filtered patches to their original positions, and combine them using suitable weights. It is worth noting that the above approach can be seen as a collaborative filtering: in general, the patches will be highly overlapped, so that each filtered pixel will result from the combination of several filtered patches. In [111], the final BM3D filter is obtained by repeating the above processing flow in a two iteration procedure. In the first step, wavelet domain denosing is achieved by simple hard-thresholding, in order to yield a coarsely denoised image. The second step uses the denoised image obtained after the first step to improve the 3-D grouping accuracy, and replaces hard-thresholding with Wiener filtering, where the energy spectrum of the noise-free image is estimated form the coarsely denoised image.

In order to adapt the BM3D filter to the case of SAR images, the SAR-BM3D filter considers two main modifications: 1) the similarity measure between patches is computed according

to (37), following the same approach as in [108]; hard-thresholding and Wiener filtering are replaced with a local linear minimum mean square error (LLMMSE) estimator [78] based on the additive signal-dependent noise model in (25). According to the two step procedure of the original BM3D filter, in the first step the LLMMSE estimator is based only on the observed image g and the filtered wavelet coefficients are obtained according to equation (27), whereas in the second step it approximates the moments of the noise-free image according to the output of the first step, and the filtered wavelet coefficients are obtained according to

$$\hat{W}_f(n) = \frac{\hat{W}^2_{f,1}(n)}{\hat{W}^2_{f,1}(n) + \sigma^2_{W_v}} W_g(n) \tag{39}$$

where $\hat{W}_{f,1}$ are the noise-free wavelet coefficients estimated at the first step and the variance of the wavelet coefficients of the signal-dependent noise is obtained as

$$\sigma^2_{W_v} = \frac{1}{|G|} \sum_{k \in G} \left[W_g(k) - \hat{W}_{f,1}(k) \right]^2 \tag{40}$$

with G denoting the set of wavelet coefficients belonging to a 3-D group. The final despeckled image is obtained as a weighted average of the overlapped denoised patches, where the weights for each patch are inversely proportional to the corresponding value of $\sigma^2_{W_v}$ [109].

An example of the application of the SAR-BM3D filter to the COSMO-SkyMed image in Fig. 10-(a) is given in 11-(b).

VII. Total Variation Regularization

Image denoising through TV regularization can be defined as the solution of a minimization problem

$$\hat{f} = \arg\min_f J(f, g) \tag{41}$$

where the cost function to be optimized can be expressed as

$$J(f, g) = \Phi(f) + \lambda \Psi(f, g). \tag{42}$$

In the above equation, $\Phi(f)$ denotes a *regularization* term including prior information about the noise-free image f, whereas $\Psi(f, g)$ denotes a *data fidelity* term.

The regularization term is usually defined as the TV norm of the noise-free image, i.e.

$$\Phi(f) = \sum_n |\nabla f(n)| \tag{43}$$

where $|\nabla f(n)|$ denotes the magnitude of the gradient of f and can be computed as

$$|\nabla f(n)| = \sqrt{f_x(n)^2 + f_x(n)^2} \tag{44}$$

where $f_x(n)$ and $f_y(n)$ denotes horizontal and vertical first order differences evaluated at pixel n, respectively. The minimization of the TV norm tends to promote a piecewise smooth image, which is usually a good prior for natural images, since it preserves important structures like edges.

The data fidelity term can be defined according to several different approaches. A popular approach is to set the data fidelity term equal to the negative of the log-likelihood of f given the observed image g, that is

$$\Psi(f, g) = -\log p(f|g). \tag{45}$$

If the TV norm is interpreted as a negative log-prior term, i.e., $\Phi(f) = -\log p(f)$, it is evident that the solution of the problem in (41) is equivalent to the MAP estimate of f.

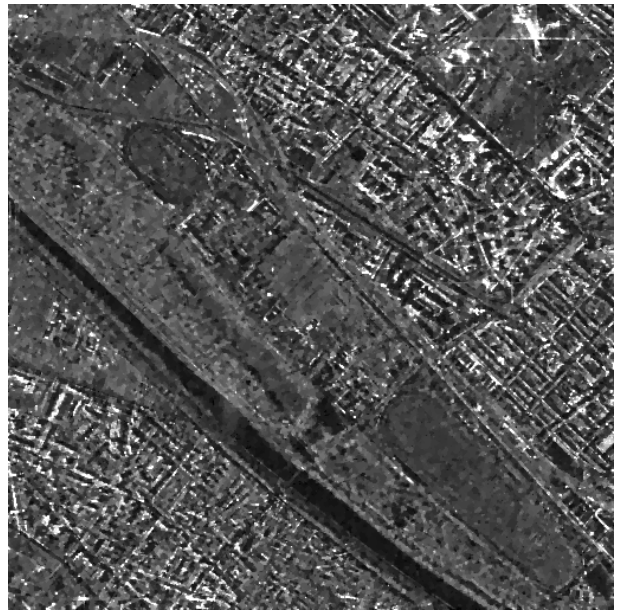

Fig. 12. Example of the application of the TV filter in [122] to the 4-look COSMO-SkyMed image in Fig. 10-(a).

A. Despeckling using TV Regularization

When it comes to despeckling, the main problem is adapting the TV framework to the multiplicative noise model. In [119], the above problem is tackled in the original intensity domain by assuming a Gamma-distributed speckle, which in turn implies a Gamma $p(f|g)$. The resulting problem can be expressed as

$$\hat{f} = \arg\min_f \sum_n |\nabla f(n)| + \lambda \sum_n \left(\log f(n) + \frac{g(n)}{f(n)} \right). \tag{46}$$

Despite its elegance, the above approach suffers from the fact that the functional is convex only for $0 < f < 2g$. In order to obtain a convex problem, several authors have considered the logarithmic domain. A simple solution is to keep the same data fidelity term as in (46), but to replace f by $f' = \log f$ in the regularization term [120], which yields

$$\hat{f}' = \arg\min_{f'} \sum_n |\nabla f'(n)| + \lambda \sum_n \left(f'(n) + g(n) e^{-f'(n)} \right). \tag{47}$$

Another natural solution is to consider a quadratic data fidelity term [117], [120], which yields

$$\hat{f}' = \arg\min_{f'} \sum_n |\nabla f'(n)| + \lambda \sum_n \left(f'(n) - g'(n) \right)^2. \tag{48}$$

Interestingly, the above solution is still equivalent to a MAP estimate when we can approximate the logarithmically transformed speckle as Gaussian.

All of the above approaches consider solutions in the spatial domain. In [122], Durand *et al.* propose to combine the advantages of the TV regularization framework with those offered by a sparse representation. The proposed solution consists in computing the data fidelity term in the domain of a redundant multiscale representation. The rationale is that relevant structures in the image are more effectively preserved in a multiscale representation, while a TV prior helps in removing characteristic artifacts caused by wavelet thresholding. In order to limit the effects of noisy wavelet coefficients, the authors of [122] propose to compute the data fidelity term on a hard-thresholded version of the observed coefficients, where the coefficients are obtained by applying a curvelet transform to the log-transformed intensity image. The authors also suggest using an underoptimal threshold, so as to preserve as much as possible curvelet coefficients relevant to edges and textures. In order to take into account the long tailed distribution of curvelet coefficients, the data fidelity term is defined as the mean absolute error between the despeckled coefficients and the hard-thresholded coefficients. The final optimization problem can be expressed as

$$\hat{f}' = \arg\min_{f'} \sum_n |\nabla f'(n)| + \lambda \sum_n |W_{f'}(n) - H[W_{g'}(n)]| \tag{49}$$

where $H[\cdot]$ denotes the hard-thresholding operator. Since the above estimator is prone to bias, the authors of [122] propose to compute the despeckled image as $\hat{f} = \exp(\hat{f}')(1 + \phi_1(L)/2)$, where $\phi_1(L)$ is the first-order polygamma function and represents the variance of L-look log-transformed speckle [33].

In general, the solution of the aforementioned optimization problems requires a suitable minimization scheme. According to the properties of the functional to be minimized, several schemes can be used, including gradient projection [118], iterative splitting methods [122], [123], inverse scale space flow [120]. The details of such minimization schemes are beyond the scope of this tutorial and the related literature is really vast. The interested reader is referred to the above cited papers and the references therein.

An example of the application of the filter proposed in [122] to the COSMO-SkyMed image in Fig. 10-(a) is given in Fig. 12.

VIII. Assessment of Despeckling Filters

One of the most challenging tasks is the validation and quality assessment of data processed for speckle reduction. The most evident problem is that the noise-free reflectivity that we wish to estimate is unknown, so that no comparison can be carried out between the output of the despeckling process and the actual *ground truth*. Another important issue is the relationship between quality and fidelity of despeckled SAR data. Like many other denoising frameworks, the quality of a processed SAR image is usually evaluated in terms of blurring of homogeneous areas, i.e., suppression of speckle noise, and detail preservation in heterogeneous areas. Nonetheless, in incoherent SAR imagery, a fundamental part of the information is represented by the relative values of the reflectivity of the targets, which allow measurements and inferences on the target scene. Consequently, the radiometric preservation of the signal is an important requirement: a good despeckling filter should not introduce bias on the reflectivity.

An immediate and subjective approach for quality assessment is represented by visual inspection of filtered images. Visual inspection permits detection of the main *human–visible* features that characterize the behavior of a despeckling filter. Such features include edge preservation capability, degree of blur, point target preservation, as well as structural artifacts which are hardly detected by objective and direct measurements. On the other hand, visual assessment does not allow either quantitative comparisons between the performances of different despeckling filters to be made or the bias introduced by the filter to be effectively estimated.

In order to overcome the limitations of visual comparison, several objective performance indexes have been proposed in the literature for the quality assessment of despeckling filters. They can be mainly divided into two classes: *with–reference* and *without–reference* indexes.

With–reference indexes are commonly used in the image denoising field. Their use implies that the noise–free, or *reference*, image is known. A typical approach consists in choosing a reference image, either optical or synthetic, representing the actual reflectivity or *ground–truth*, and creating a *synthetically* degraded version according to a given signal model. These indexes permit a quantitative and objective comparison between the performances of different filters, which are expected to perform similarly on real SAR images. Moreover, insights on filters behavior on specific image features, like edge preservation and homogeneous areas smoothing, can be easily highlighted by choosing appropriate reference images and even synthetic–generated patterns. Unfortunately, experimental results carried out on simulated SAR images often are not sufficient to infer the performances of despeckling filters on real SAR images, since the synthetically speckled image may not be consistent with the actual SAR image formation and acquisition processes. Furthermore, the statistical properties of the chosen reference image and of a real ground–truth reflectivity can substantially differ.

On the contrary, without–reference indexes do not trust on the knowledge of the ground–truth. They are uniquely based on specific statistical hypotheses on the signal model. Since the signal model is strongly dependent on the degree of scene heterogeneity, a supervised selection of the most appropriate areas for the computation of a specific index, e.g., homogeneous areas, may be required.

In the following, the most used indexes belonging to both the above mentioned classes are presented. Note that the statistical operator of expectation $E[\cdot]$ and the moments of the involved variables, such as the variance and covariance, here denoted as $\mathrm{Var}[\cdot]$ and $\mathrm{Cov}[\cdot]$ for the sake of simplicity, should be replaced by their empirical versions based on spatial averages when evaluating the indexes.

A. With–reference indexes

The mean square error (MSE), or Euclidean distance, between the ground–truth f and the despeckled image $\hat{f}$, and

TABLE I
LIST OF COMMONLY USED WITH-REFERENCE INDEXES FOR EVALUATING PERFORMANCES OF DESPECKLING ALGORITHMS.

Index	Note
$\mathrm{MSE} = \mathrm{E}[(\hat{f} - f)^2]$	f, $\hat{f}$: speckle–free despeckled images
$\mathrm{SNR} = 10 \cdot \log_{10} \left[\frac{\mathrm{Var}[f]}{\mathrm{MSE}}\right]$	$\mathrm{Var}[f]$: speckle–free image variance
$\mathrm{PSNR} = 10 \cdot \log_{10} \left[\frac{f_{\mathrm{PEAK}}^2}{\mathrm{MSE}}\right]$	f_{PEAK}: maximum value allowed by the samples dynamic range
$\mathrm{SMSE} = 10 \cdot \log_{10} \left[\frac{\mathrm{E}[f^2]}{\mathrm{MSE}}\right]$	$\mathrm{E}[f^2]$: speckle–free image power
$\mathrm{MSSIM} = \frac{1}{M} \sum_{p=0}^{M-1} \left[\frac{2 \cdot \mathrm{E}[f_p] \cdot \mathrm{E}[\hat{f}_p] + C_1}{\mathrm{E}[f_p^2] + \mathrm{E}[\hat{f}_p^2] + C_1} \frac{2 \cdot \mathrm{Cov}[f_p, \hat{f}_p] + C_2}{\mathrm{Var}[f_p] + \mathrm{Var}[\hat{f}_p] + C_2}\right]$	f_p, $\hat{f}_p$, $p = 0, \ldots, M-1$: speckle–free and despeckled image patches; C_1, C_2: suitable constants.
$\mathrm{EC} = \frac{\mathrm{Cov}[f^H, \hat{f}^H]}{\sqrt{\mathrm{Var}[f^H] \cdot \mathrm{Var}[\hat{f}^H]}}$	f^H, $\hat{f}^H$: highpass–filtered speckle–free and despeckled images
$\mathrm{FOM} = \frac{1}{\max(\hat{N}, N)} \sum_{n=1}^{\hat{N}} \frac{1}{1 + d_n^2 \alpha}$	N, $\hat{N}$: number of points belonging to an edge in speckle–free and despeckled image patches; d_n^2: Euclidean distance between the edge pixels in the despeckled image patch and the nearest ideal edge pixel in the speckle–free one; α: suitable constant.

other measures derived from the MSE, like the signal–to–noise ratio (SNR), the peak signal–to–noise ratio (PSNR) and the signal–to–mean square error (SNRS), have been widely used for the quality assessment of both denoising and despeckling [33], [57], [76]. Unlike the case of additive signal–independent noise, in the presence of signal–dependent noise the MSE is strongly influenced by the average signal level of the ground truth. Consequently, a quantitative evaluation of despeckling filters using this kind of indexes is strongly dependent on the content of the ground–truth image, even though performance hierarchy is usually preserved across different images.

MSE–based measurements are useful to obtain a global performance assessment on the whole image, but usually they yields little information about the preservation of specific features, for which other indexes can be used. The *mean structural similarity index measurement* (MSSIM) [135], proposed for the general denoising framework and adopted also in the context of despeckling, underlines the perceived changes in structural information after the filtering process. MSSIM takes values over the interval $[0, 1]$, where 0 and 1 indicate no structural similarity and perfect similarity, respectively. As demonstrated in [135], MSSIM can substantially differ between images having very similar MSE values.

The *edge correlation* (EC) index has been proposed as a measure of edge preservation for despeckling of echographic images [136] and has been extended to the SAR field [72]; it is defined as the correlation coefficient ($0 \leq \mathrm{EC} \leq 1$) between highpass versions of the original and despeckled images. This index may be distorted by possible residual speckle noise that is enhanced by the highpass filtering.

Another index of edge preservation is Pratt's *figure of merit* (FOM), which has been used in [96] for the quality assessment of despeckled SAR and ultrasound images. FOM is defined on a local patch of the image containing an edge. The more similar the edge maps, the closer to zero the FOM values. Consequently, this index is strictly related to the map edge detector that is used, which is crucial especially for the despeckled image when a residual noise component is present.

Table I summarizes the above mentioned indexes.

A synthetically speckled images has been produced starting from a 512×512 digitized aerial photograph of San Francisco. The original speckle-free image, regarded as an amplitude format, has been squared and multiplied by an exponentially distributed fading term, in order to simulate a single-look SAR image in intensity format. The simulated speckle is spatially uncorrelated and fully developed. The noisy intensity image, together with all filtered intensity versions, has been square rooted, for displaying convenience, and is shown together with the 8-bit original, regarded as an amplitude image, in Fig. 13-(b) and Fig. 13-(a), respectively.

The filters compared in this subsection are representative of different approaches to despeckling described in this paper: Kuan [52] and Γ–MAP [54] as classical spatial filters; GG–MAP–S [83] and LG–MAP–C [85] as Bayesian filters in the wavelet domain (input format is square root of intensity [137]); Probability Patch–Based (PPB) [108] and SAR–BM3D [109] as non–local mean filters in the spatial and wavelet domain; L1 Fidelity on Frame Coefficients (L1–FFC) [122] as a TV-based filter. Visual comparisons of the results obtained with the same filters can be made observing Fig. 13. What immediately stands out is that local spatial filter (Kuan and Γ–MAP) are unable to clean the noisy background. A residual inhomogeneity, like a coarse granular texture, is noticeable especially on the sea. This effect is thoroughly missing in wavelet-domain filters, as well as in nonlocal-mean and TV filters. Preprocessing of point targets was disabled in wavelet schemes, because the simulated speckle is fully developed.

Fig. 14 shows the performance indexes obtained by means of the test despeckling filters.

B. Without–reference indexes

As previously stated, without–reference indexes do not rely on the complete knowledge of the true reflectivity, but are based on the statistical model of the SAR signal as well as on some simple assumptions on the degree of heterogeneity of the underlying scene.

The *equivalent number of look* (ENL) [46] is an index suitable for evaluating the level of smoothing in homogeneous areas, that is where the scene variation is supposed to be negligible with respect to speckle noise fluctuations. The ENL of the original SAR image corresponds to the nominal number

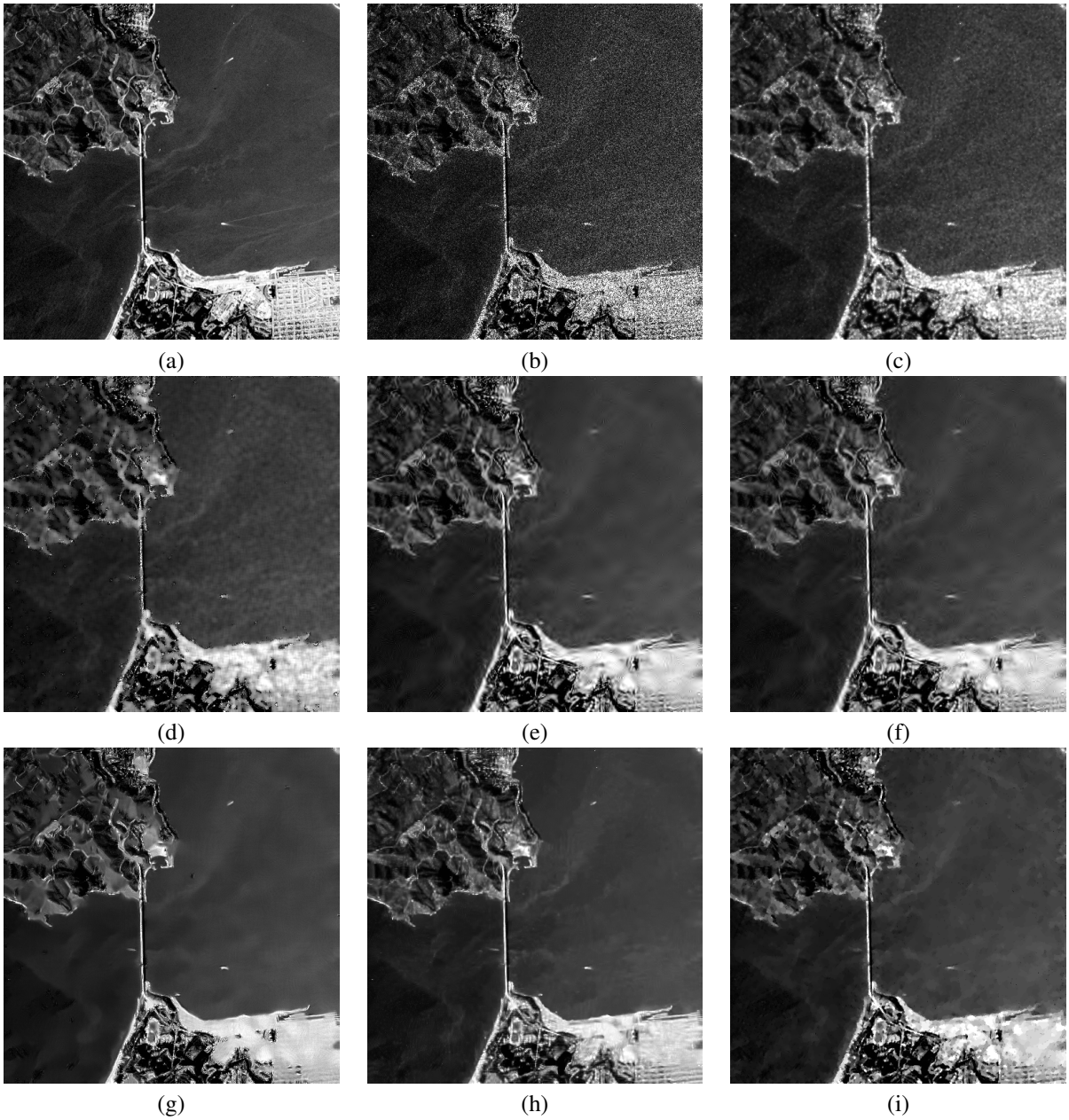

Fig. 13. Results on a synthetically speckled image: (a) noise-free reference; (b) noisy (1-look); (c) Kuan; (d) Γ-MAP; (e) GG–MAP–S; (f) LG–MAP–C; (g) PPB; (h) SAR–BM3D; (i) L1–FFC.

of looks, whereas it increases after the despeckling stage according to the smoothing capability of the filter.

Other typical measures can be computed from the *ratio image* r, defined as the point–by–point ratio between the noisy and the filtered image [4]

$$r(n) = \frac{g(n)}{\hat{f}(n)}. \tag{50}$$

The ratio image is a useful information in both homogeneous and heterogeneous scenes, wherever the fully developed speckle model holds. It represents the noise pattern removed by the despeckling filter that, according to the model, should be Γ-distributed. An ideal filter should result in a pure random pattern, whereas poor speckle noise removal causes structural information, such as borders and edges, to be clearly visible in the ratio image. The mean and the variance of r, that is $\mu_r = \mathrm{E}[r]$ and $\sigma_r^2 = \mathrm{Var}[r]$, should be as close as possible to the respective theoretical statistical moments of the speckle noise process. For this reason, they are often used as indexes of bias and speckle power suppression, respectively. A *measure of bias* is also given by the B index [30], in which a value close to zero indicates an unbiased estimation.

Under the hypothesis of multiplicative speckle noise, a measure of texture preservation on heterogeneous areas is given by the comparison between the *coefficient of variation* calculated on the despeckled image, namely $C_{\hat{f}}$, and its the expected theoretical value on the noise-free image, C_f [20]. Intuitively, a poor preservation of details yields $C_f > C_{\hat{f}}$, while the introduction of impairments leads to $C_f < C_{\hat{f}}$.

Since the speckle model does not hold in the presence

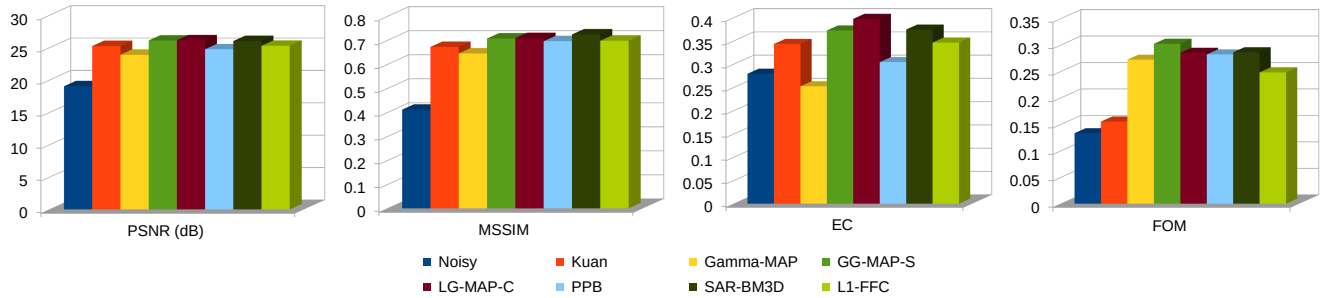

Fig. 14. With-reference indexes computed for the image in Fig. 13-(b), with the image Fig. 13-(a) as speckle–free reflectivity.

TABLE II
LIST OF COMMONLY USED WITHOUT-REFERENCE INDEXES FOR EVALUATING PERFORMANCES OF DESPECKLING ALGORITHMS.

Index	Note
$\mathrm{ENL} = \frac{\mathrm{E}[\hat{f}]^2}{\mathrm{Var}[\hat{f}]}$	f, $\hat{f}$: speckle–free and despeckled images; ENL is evaluated in homogeneous areas
$\mu_r = \mathrm{E}[r]$, $\sigma_r^2 = \mathrm{Var}[r]$	$r(n) = \frac{g(n)}{\hat{f}(n)}$: ratio image
$\mathrm{B} = \mathrm{E}\left[\frac{(g-\hat{f})}{g}\right]$	
$\mathrm{C}_{\hat{f}} = \frac{\sqrt{\mathrm{Var}[\hat{f}]}}{\mathrm{E}[\hat{f}]}$	$\mathrm{C}_f = \sqrt{\frac{C_g^2 - C_u^2}{1+C_u^2}}$ (expected value); C_g, C_u: coefficients of variation of the observed noisy image g and of the speckle noise u
$\mathrm{TCR} = 20\log_{10}\frac{\max_{\mathcal{P}}[g]}{\mathrm{E}_{\mathcal{P}}[g]}$	$\mathcal{P}$: patch containing a point target; $\max_{\mathcal{P}}$, $\mathrm{E}_{\mathcal{P}}$ computed over the patch

of persistent scatterers or point targets, despeckling filters should keep their values unchanged. A point target is usually characterized by a cluster of pixels whose reflectivity values are much higher, even some orders of magnitude, than the mean reflectivity of the surrounding scene. The *target–to–clutter ratio* (TCR) [138], [139] aims at measuring the relative value of strong scatterers with respect to the values of the surrounding pixels. TCR values computed before and after despeckling are indicative about how much a filter preserves the radiometric properties in the patch.

Table II summarizes the most commonly used without-reference indexes for evaluating despeckling algorithms performance. Fig. 15 shows the without–reference indexes obtained on the image in Fig. 10-(a). The indexes have been computed for the original 1024×1024 image and for a 512×512 4–look version, generated by means of spatial multilooking (2×2 average).

C. Discussion

The computational complexities of the most relevant filters among those reviewed raises an interesting concern. Early spatial filters are nowadays real-time (less than 1 s to process a 1024×1024 scene on a standard platform). Wavelet-based methods are at least ten times longer to run, up to one hundred times for GG–MAP–S, which requires numerical calculation of the maximum of a function [83], unlike LMMSE and LG–MAP–C, which admit closed form solutions. For all multiresolution methods, biorthogonal 9/7 wavelet filters and four levels of decomposition (corresponding to a baseband approximation having 4^4=256 nominal looks) have been used. Biorthogonal filters are preferred to orthogonal filters in image processing applications because they allow filters of different lengths, and hence of spectral selectivity, to be available for the lowpass (9 coeffs.) and highpass (7 coeffs.) analyses. Conversely, NL filtering approaches, in either space (PPB) or wavelet (SAR–BM3D) domain, have a significantly higher computational cost, mainly because of iterated processing, with recalculation of statistics after each step. Eventually, the TV-based filter examined (L1–FFC) is comparable with NL filters. The numbers of iterations are those recommended by the respective authors in their implementations. Table III summarizes the complexity of despeckling algorithms.

A key point in the despeckling of SAR images is the extent to which models assumed for the signal or the noise match the actual statistics of the data. By observing the results on 1-look data in Fig. 15, it is quite evident that all filters yield a biased outcome ($\mu_r < 1$, $B > 1$) and a limited speckle removal capability ($\sigma_r^2 < 1$): Both these effects occur because all filters do not take into account that speckle is spatially autocorrelated in real single–look SAR images [30], for the following reasons: 1) oversampling of SAR raw data with respect to the Nyquist rate given by twice the chirp bandwidth; 2) frequency windowing applied when the raw data are focused and aimed at improving the response of targets, avoiding Gibbs' effects. As reported in Fig. 15 for 4-looks data, multilooking allows all filters to obtain values of μ_r and σ_r^2 closer to the ideal ones. This mainly happens because the multilooking process reduces the speckle correlation; unfortunately, it also halves the image resolution in both range and azimuth directions.

Very few despeckling filters that specifically consider the speckle correlation have been proposed in the literature (e.g., [30]). Recently, a blind speckle decorrelation method to be applied to SLC images has been proposed [31], [140] to

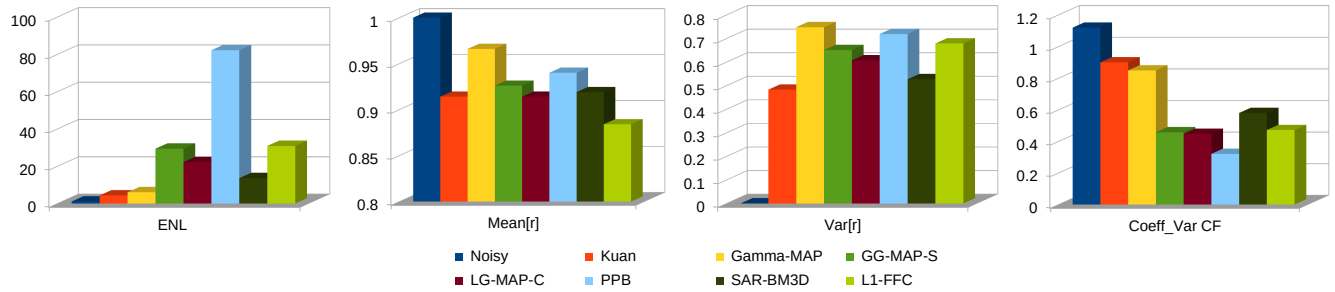

(a)

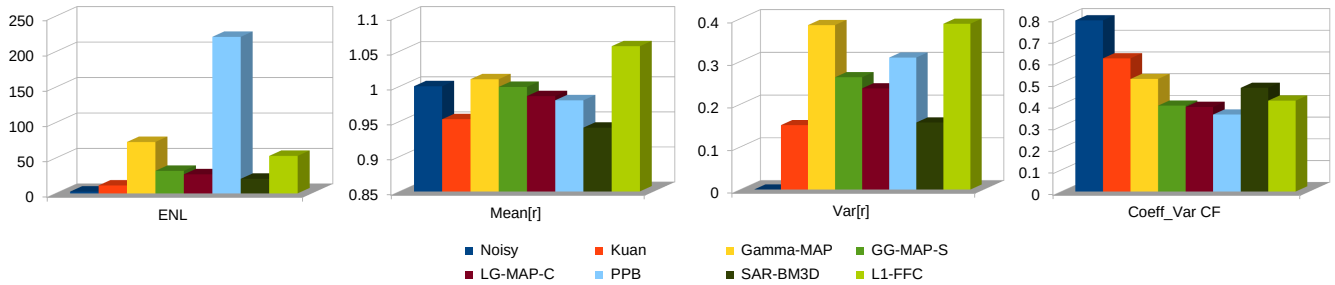

(b)

Fig. 15. Without-reference indexes computed for different despeckling algorithms for the image in Fig. 10-(a). (a) one-look image (theoretical value $C_f = 0.355$); (b) 4-look version of the same image (theoretical value $C_f = 0.544$).

enhance the performances of existing despeckling filters. The idea is estimating the SAR system frequency response on the original SLC image in order to compensate its effect by an inverse filtering (*whitening stage*), so that an SLC image having uncorrelated speckle noise, but preserving the radiometric features, is produced. In [141], it has been shown that the introduction of the whitening stage allows noticeable performance gains for filters based on the uncorrelated speckle model. A visual and numerical example on a single–look COSMO–SkyMed image is proposed in Fig. 16. The correlation coefficient ρ dramatically decreases after the whitening stage. MAP–GG–S outperforms its own results when it is applied to the uncorrelated speckled image. The problem of speckle correlation occurs only for one-look data, because the process of multilooking, equivalent to lowpass filtering and decimation, lowers the correlation coefficient (CC) of speckle from about 35% to less than 10% [142].

A visual analysis of the image details in Fig. 16 highlights that wavelet despeckling suffers from the presence of structured artifacts mainly located around edges, referred to as *glitches*, that are due, in order of importance, to: 1) speckle correlation, 2) input image format (amplitude, is preferable to intensity, because yields a more accurate MAP estimation in UDWT domain [143]), 3) type of wavelet filter (the shortest filters of Haar transform [89] produce the least noticeable artifacts). Also the type of decomposition (à trous wavelet (ATWT) [37] rather than UDWT) is a topic worth being investigated, also because ATWT accommodates all details of one scale in a unique plane; thus the number of coefficients to be despeckled, and hence computing times, would be three times lower. However, the adaptivity with orientation featured by UDWT would be lost with ATWT.

The assessment of the performances of despeckling filters on real SAR data is often problematic due to the lack of with–reference indexes. In order to overcome such problems, a possible idea is to use electromagnetic SAR image generators [23]. Such simulators are based on more physical–oriented models, which consider the propagation of the electromagnetic wave and its interaction with targets and surfaces, and usually require a more detailed parametric description of the target scene with respect to the models used in signal processing applications. In [22], the authors use an electromagnetic SAR image generator to simulate several independent acquisitions of the same scene. If the number of acquisitions is sufficiently high, their average can be considered as a good approximation of the noise–free reflectivity and can be used to compute with–reference indexes. The advantage of this technique is that the simulated images do not necessarily obey the fully developed speckle model and provide insights on the behavior of the filter on point targets and highly heterogeneous areas. On the other hand, the underlying reflectivity follows a synthetically generated pattern, which may not be fully representative of the reflectivity usually encountered in real SAR images, especially in complex scenes, due to the ideal models of objects fed to the simulator.

Another viable approach to devise a fully automatic method for quality assessment of despeckled SAR images was recently proposed by the authors [144]. The rationale of the new approach is that any structural perturbation introduced by despeckling, e.g., a local bias of mean or the blur of a sharp edge or the suppression of a point target, may be regarded either as the introduction of a new structure or as the suppres-

TABLE III
COMPUTATIONAL COMPLEXITY OF DESPECKLING METHODS. BETWEEN TWO CONSECUTIVE GRADES THERE IS APPROXIMATELY ONE ORDER OF MAGNITUDE. SO, PPB IS ABOUT 1000 TIMES SLOWER THAN KUAN'S FILTER, ON THE SAME COMPUTING PLATFORM.

FIlter	Kuan (7×7)	Γ–MAP (7×7)	UDWT LMMSE	LG–MAP–C	GG–MAP–S	PPB	SAR–BM3D	L1–FFC
Complexity	Very low	Very Low	Low	Low	Medium	High	High	High

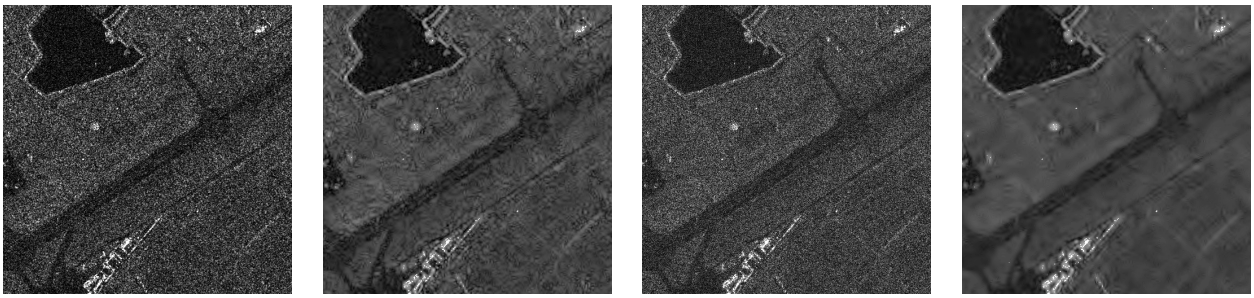

(a) (b) (c) (d)

Fig. 16. (a) original one-look COSMO-SkyMed image ($\rho \simeq 0.29$); (b) MAP–GG–S [83] of original (ENL = 27.90, $\mu_r = 0.940$, $\sigma_r^2 = 0.702$); (c) whitened [141] ($\rho \simeq 0.05$); (d) MAP–GG–S of whitened (ENL = 142.29, $\mu_r = 0.997$, $\sigma_r^2 = 0.936$). ρ is the CC of speckle measured on the complex image [29]; ENL, μ_r and σ_r^2 are calculated on a homogeneous patch after despeckling.

sion of an existing one. Conversely, plain removal of random noise does not change structures in the image. Structures are identified as clusters in the normalized scatterplot of original to filtered image. Ideal filtering should produce clusters all aligned along the main diagonal. In practice clusters are moved far from the diagonal. Cluster centers are detected through the *mean shift* algorithm. A structural change feature is defined at each pixel from the position and population of off-diagonal clusters [145]. Such a feature may be regarded as a spatial map of filtering inaccuracies. A preliminary validation has been carried out on simulated SAR images, with a good correlation between feature and objective filtering error. In experiments on COSMO-SkyMed images, the automatic ranking of filters matches the subjective trials of experts. The proposed feature detects filtering impairments but is unable to measure the overall effectiveness of filtering. Therefore, its use must be coupled with another index measuring the effectiveness of cleaning, e.g., ENL, regardless of its accuracy.

IX. CONCLUSIONS AND PERSPECTIVES

This tutorial has demonstrated that despeckling of SAR images takes into account several issues related to signal and noise modeling, signal representation, estimation theory and quality assessment. Concerning Bayesian estimation, starting from Lee filter, local-window adaptive filtering has been progressively enhanced, up to a saturation of performances, due to the trade off of using windows small enough to retain edges textures and fine details and large enough to allow a consistent and confident statistical estimate to be achieved.

In the last two decades, the introduction of multiresolution analysis has been found to boost despeckling algorithms performances. Key points of wavelet-based despeckling is the modeling of the reflectivity and of the signal-dependent noise in the wavelet domain and the choice of the estimation criterion to achieve the noise-free wavelet coefficients. While several authors have chosen overfitting models sacrificing space adaptivity, others have tried to keep the advantages of an adaptivity in both scale and space by using pdf with few parameters to be estimated locally on subbands/frames. A preprocessing step of point targets that must retain their radiometry after despeckling and a *segmented* approach, in which sample statistics are calculated on homogeneous segments, complete Bayesian despeckling in wavelet domain.

As to non-Bayesian approaches, Lee's sigma filter has evolved into bilateral filtering, which has possibly inspired nonlocal filtering, excellent examples of which are found both in spatial and in wavelet domains. In parallel, total variation has emerged as a powerful regularization technique that can be specialized to the signal dependent noise model and allows constraints to be set on several mathematical properties of the output image. As an example, setting a constraint on L1 norm definitely avoids glitches and other impairments. Presently, computational issues are mainly responsible for the moderate, yet increasing, popularity of such methods among users.

New horizons are undoubtedly in the direction of *compressed sensing*, of which denoising seems to be one of the most promising application, notwithstanding objective difficulties come from the signal dependent, and hence nonstationary, noise model. Given the huge effort of researchers in this area, new developments and applications to despeckling are expected in a near future. Computational issues are also the main drawback of algorithms based on compressed sensing, with respect to spatial and wavelet domain Bayesian algorithms. The ever increasing diffusion of multiprocessor systems will be beneficial for methods that can be easily parallelized.

X. ACKNOWLEDGMENTS

The authors are grateful to C. Deledalle and to L. Verdoliva for providing us the codes of PPB and SAR-BM3D methods, respectively. The COSMO-SkyMed data were kindly made available by the Italian Space Agency (ASI).

References

[1] A. Moreira, P. Prats-Iraola, M. Younis, G. Krieger, I. Hajnsek, and K. P. Papathanassiou, "A tutorial on synthetic aperture radar," *IEEE Geosci. Remote Sens. Mag.*, vol. 1, no. 1, pp. 6–43, Mar. 2013.

[2] L. Alparone, S. Baronti, A. Garzelli, and F. Nencini, "Landsat ETM+ and SAR image fusion based on generalized intensity modulation," *IEEE Trans. Geosci. Remote Sens.*, vol. 42, no. 12, pp. 2832–2839, Dec. 2004.

[3] F. Argenti, G. Torricelli, and L. Alparone, "MMSE filtering of generalised signal-dependent noise in spatial and shift-invariant wavelet domains," *Signal Process.*, vol. 86, no. 8, pp. 2056–2066, Aug. 2006.

[4] C. Oliver and S. Quegan, *Understanding Synthetic Aperture Radar Images*, Artech House, Boston, MA, 1998.

[5] L. M. Novak and M. C. Burl, "Optimal speckle reduction in polarimetric SAR imagery," *IEEE Trans. Aerosp. Electron. Syst.*, vol. 26, no. 2, pp. 293–305, Mar. 1990.

[6] Jong-Sen Lee, M. R. Grunes, and S. A. Mango, "Speckle reduction in multipolarization, multifrequency SAR imagery," *IEEE Trans. Geosci. Remote Sens.*, vol. 29, no. 4, pp. 535–544, Jul. 1991.

[7] R. Touzi and A. Lopès, "Principle of speckle filtering in polarimetric SAR imagery," *IEEE Trans. Geosci. Remote Sens.*, vol. 32, no. 5, pp. 1110–1114, Sep. 1994.

[8] Jong-Sen Lee, M. R. Grunes, and G. De Grandi, "Polarimetric SAR speckle filtering and its implication for classification," *IEEE Trans. Geosci. Remote Sens.*, vol. 37, no. 5, pp. 2363–2373, Sep. 1999.

[9] Jong-Sen Lee, M. R. Grunes, D. L. Schuler, E. Pottier, and L. Ferro-Famil, "Scattering-model-based speckle filtering of polarimetric SAR data," *IEEE Trans. Geosci. Remote Sens.*, vol. 44, no. 1, pp. 176–187, Jan. 2006.

[10] R. J. Dekker, "Speckle filtering in satellite SAR change detection images," *Int. J. Remote Sens.*, vol. 19, no. 6, pp. 1133–1146, Apr. 1998.

[11] S. Quegan and Jiong Jiong Yu, "Filtering of multichannel SAR images," *IEEE Trans. Geosci. Remote Sens.*, vol. 39, no. 11, pp. 2373–2379, Nov. 2001.

[12] J. Bruniquel and A. Lopès, "Multivariate optimal speckle reduction in SAR imagery," *Int. J. Remote Sens.*, vol. 18, no. 3, pp. 603–627, Feb. 1997.

[13] R. Touzi, A. Lopès, J. Bruniquel, and P. W. Vachon, "Coherence estimation for SAR imagery," *IEEE Trans. Geosci. Remote Sens.*, vol. 37, no. 1, pp. 135–149, Jan. 1999.

[14] P. A. Rosen, S. Hensley, I. R. Joughin, F. K. Li, S. N. Madsen, E. Rodriguez, and R. M. Goldstein, "Synthetic Aperture Radar interferometry," *Proc. IEEE*, vol. 88, no. 3, pp. 333–382, Mar. 2000.

[15] Jong-Sen Lee, K. P. Papathanassiou, T. L. Ainsworth, M. R. Grunes, and A. Reigber, "A new technique for noise filtering of SAR interferometric phase images," *IEEE Trans. Geosci. Remote Sens.*, vol. 36, no. 5, pp. 1456–1465, Sep. 1998.

[16] B. Aiazzi, S. Baronti, M. Bianchini, A. Mori, and L. Alparone, "Filtering of interferometric SAR phase images as a fuzzy matching-pursuit blind estimation," *EURASIP J. Appl. Signal Process.*, vol. 2005, no. 20, pp. 3220–3230, 2005.

[17] M. Costantini, "A novel phase unwrapping method based on network programming," *IEEE Trans. Geosci. Remote Sens.*, vol. 36, no. 3, pp. 813–821, May 1998.

[18] B. Aiazzi, L. Alparone, S. Baronti, and A. Garzelli, "Coherence estimation from incoherent multilook SAR imagery," *IEEE Trans. Geosci. Remote Sens.*, vol. 41, no. 11, pp. 2531–2539, Nov. 2003.

[19] Jong-Sen Lee, I. Jurkevich, P. Dewaele, P. Wambacq, and A. Oosterlinck, "Speckle filtering of synthetic aperture radar images: a review," *Remote Sens. Rev.*, vol. 8, no. 4, pp. 313–340, 1994.

[20] R. Touzi, "A review of speckle filtering in the context of estimation theory," *IEEE Trans. Geosci. Remote Sens.*, vol. 40, no. 11, pp. 2392–2404, Nov. 2002.

[21] Jong-Sen Lee, "Digital image enhancement and noise filtering by use of local statistics," *IEEE Trans. Pattern Anal. Mach. Intell.*, vol. PAMI-2, no. 2, pp. 165–168, Feb. 1980.

[22] G. Di Martino, M. Poderico, G. Poggi, D. Riccio, and L. Verdoliva, "Benchmarking framework for SAR despeckling," *IEEE Trans. Geosci. Remote Sens.*, Article in Press.

[23] G. Franceschetti, M. Migliaccio, D. Riccio, and G. Schirinzi, "SARAS: a synthetic aperture radar SAR raw signal simulator," *IEEE Trans. Geosci. Remote Sens.*, vol. 30, no. 1, pp. 110–123, Jan. 1992.

[24] C. Elachi and J. J. van Zyl, *Introduction To The Physics and Techniques of Remote Sensing*, John Wiley & Sons, Hoboken, NJ, 2006.

[25] F. T. Ulaby, R. K. Moore, and A. K. Fung, *Microwave Remote Sensing: Active and Passive, Volume II: Radar Remote Sensing and Surface Scattering and Emission Theory*, Artech House, Norwood, MA, 1986.

[26] J. W. Goodman, "Some fundamental properties of speckle," *J. Opt. Soc. Am.*, vol. 66, no. 11, pp. 1145–1150, Nov. 1976.

[27] M. Tur, K. C. Chin, and J. W. Goodman, "When is speckle multiplicative?," *Appl. Optics*, vol. 21, no. 7, pp. 1157–1159, Apr. 1982.

[28] J. C. Curlander and R. N. McDonough, *Synthetic Aperture Radar: Systems & Signal Processing*, John Wiley & Sons, New York, 1991.

[29] S. N. Madsen, "Spectral properties of homogeneous and nonhomogeneous radar images," *IEEE Trans. Aerosp. Electron. Syst.*, vol. AES-23, no. 4, pp. 583–588, Jul. 1987.

[30] S. Solbø and T. Eltoft, "A stationary wavelet-domain Wiener filter for correlated speckle," *IEEE Trans. Geosci. Remote Sens.*, vol. 46, no. 4, pp. 1219–1230, Apr. 2008.

[31] A. Lapini, T. Bianchi, F. Argenti, and L. Alparone, "A whitening method for the despeckling of SAR images affected by correlated speckle noise," in *Proc. 20th European Signal Processing Conf. (EUSIPCO)*, 2012, pp. 2487–2491.

[32] H. H. Arsenault and M. Levesque, "Combined homomorphic and local-statistics processing for restoration of images degraded by signal-dependent noise," *Appl. Optics*, vol. 23, no. 6, pp. 845–850, Mar. 1984.

[33] H. Xie, L. E. Pierce, and F. T. Ulaby, "Statistical properties of logarithmically transformed speckle," *IEEE Trans. Geosci. Remote Sens.*, vol. 40, no. 3, pp. 721–727, Mar. 2002.

[34] I. Daubechies, "Orthonormal bases of compactly supported wavelets," *Commun. Pur. Appl. Math.*, vol. 41, pp. 909–996, 1988.

[35] S. Mallat, "A theory for multiresolution signal decomposition: the wavelet representation," *IEEE Trans. Pattern Anal. Mach. Intell.*, vol. PAMI-11, no. 7, pp. 674–693, Jul. 1989.

[36] S. M. Kay, *Fundamentals of Statistical Processing, Volume I: Estimation Theory*, Prentice Hall, Engl. Cliffs, NJ, 1993.

[37] M. J. Shensa, "The discrete wavelet transform: wedding the à trous and Mallat algorithms," *IEEE Trans. Signal Process.*, vol. 40, no. 10, pp. 2464–2482, Oct. 1992.

[38] G. P. Nason and B. W. Silverman, "The stationary wavelet transform and some statistical applications," in *Wavelets and Statistics*, A. Antoniadis and G. Oppenheim, Eds., vol. 103 of *Lecture Notes in Statistics*, pp. 281–299. Springer-Verlag, New York, 1995.

[39] F. Argenti G. Torricelli and L. Alparone, "Signal dependent noise removal in the undecimated wavelet domain," in *Proc. IEEE Int. Conf. on Acoustics, Speech and Signal Processing (ICASSP)*, 2002, vol. 4, pp. 3293–3296.

[40] P. P. Vaidyanathan, *Multirate Systems and Filter Banks*, Prentice Hall, Engl. Cliffs, NJ, 1992.

[41] Minh N. Do and M. Vetterli, "The contourlet transform: An efficient directional multiresolution image representation," *IEEE Trans. Image Process.*, vol. 14, no. 12, pp. 2091–2106, Dec. 2005.

[42] E. Candès and D. Donoho, "Curvelets a surprisingly effective non-adaptive representation for objects with edges," in *Curves and Surface Fitting: Saint-Malo 1999*, A. Cohen, C. Rabut, and L. Schumaker, Eds. 2000, pp. 105–120, Vanderbilt University Press.

[43] J. L. Starck, E. J. Candès, and D. L. Donoho, "The curvelet transform for image denoising," *IEEE Trans. Image Process.*, vol. 11, no. 6, pp. 670–684, Jun. 2002.

[44] F. Argenti, T. Bianchi, G. Martucci di Scarfizzi, and L. Alparone, "LMMSE and MAP estimators for reduction of multiplicative noise in the nonsubsampled contourlet domain," *Signal Process.*, vol. 89, no. 10, pp. 1891–1901, Oct. 2009.

[45] L. Alparone, F. Argenti, T. Bianchi, and A. Lapini, "An evaluation of Bayesian estimators and PDF models for despeckling in the undecimated wavelet domain," in *SAR Image Analysis, Modeling, and Techniques X*, C. Notarnicola, Ed., 2010, vol. 7829 of *Proc. of SPIE*, pp. 782902–1–782902–12.

[46] Jong-Sen Lee, "Speckle analysis and smoothing of synthetic aperture radar images," *Comput. Graph. Image Process.*, vol. 17, no. 1, pp. 24–32, Sep. 1981.

[47] Jong-Sen Lee, "Speckle suppression and analysis for synthetic aperture radar images," *Opt. Eng.*, vol. 25, no. 5, pp. 636–643, May 1986.

[48] F. T. Ulaby, F. Kouyate, B. Brisco, and T. H. Lee Williams, "Textural information in SAR images," *IEEE Trans. Geosci. Remote Sens.*, vol. 24, no. 2, pp. 235–245, Mar. 1986.

[49] Jong-Sen Lee, "Refined filtering of image noise using local statistics," *Comput. Graph. Image Process.*, vol. 15, no. 2, pp. 380–389, Apr. 1981.

[50] V. S. Frost, J. A. Stiles, K. S. Shanmugan, and J. C. Holtzman, "A model for radar images and its application to adaptive digital filtering of multiplicative noise," *IEEE Trans. Pattern Anal. Mach. Intell.*, vol. PAMI-4, no. 2, pp. 157–166, Feb. 1982.

[51] A. Lopès, R. Touzi, and E. Nezry, "Adaptive speckle filters and scene heterogeneity," *IEEE Trans. Geosci. Remote Sens.*, vol. 28, no. 6, pp. 992–1000, Nov. 1990.

[52] D. T. Kuan, A. A. Sawchuk, T. C. Strand, and P. Chavel, "Adaptive noise smoothing filter for images with signal-dependent noise," *IEEE Trans. Pattern Anal. Mach. Intell.*, vol. PAMI-7, no. 2, pp. 165–177, Feb. 1985.

[53] D. T. Kuan, A. A. Sawchuk, T. C. Strand, and P. Chavel, "Adaptive restoration of images with speckle," *IEEE Trans. Acoust., Speech, Signal Process.*, vol. ASSP-35, no. 3, pp. 373–383, Mar. 1987.

[54] A. Lopès, E. Nezry, R. Touzi, and H. Laur, "Maximum a posteriori speckle filtering and first order texture models in SAR images," in *Proc. IEEE Int. Geoscience and Remote Sensing Symp. (IGARSS)*, 1990, pp. 2409–2412.

[55] A. Lopès, E. Nezry, R. Touzi, and H. Laur, "Structure detection and statistical adaptive speckle filtering in SAR images," *Int. J. Remote Sens.*, vol. 14, no. 9, pp. 1735–1758, Jun. 1993.

[56] A. Baraldi and F. Parmiggiani, "A refined gamma MAP SAR speckle filter with improved geometrical adaptivity," *IEEE Trans. Geosci. Remote Sens.*, vol. 33, no. 6, pp. 1245–1257, Nov. 1995.

[57] M. Walessa and M. Datcu, "Model-based despeckling and information extraction from SAR images," *IEEE Trans. Geosci. Remote Sens.*, vol. 38, no. 5, pp. 2258–2269, Sep. 2000.

[58] D. Espinoza Molina, D. Gleich, and M. Datcu, "Evaluation of Bayesian despeckling and texture extraction methods based on Gauss–Markov and auto-binomial Gibbs random fields: application to TerraSAR-X data," *IEEE Trans. Geosci. Remote Sens.*, vol. 50, no. 5, pp. 2001–2025, May 2012.

[59] B. Aiazzi, L. Alparone, and S. Baronti, "Multiresolution local-statistics speckle filtering based on a ratio Laplacian pyramid," *IEEE Trans. Geosci. Remote Sens.*, vol. 36, no. 5, pp. 1466–1476, Sep. 1998.

[60] P. Meer, R.-H. Park, and K. Cho, "Multiresolution adaptive image smoothing," *Graph. Models Image Process.*, vol. 56, no. 2, pp. 140–148, Mar. 1994.

[61] B. Aiazzi, L. Alparone, S. Baronti, and G. Borri, "Pyramid-based multiresolution adaptive filters for additive and multiplicative image noise," *IEEE Trans. Circuits Syst. II*, vol. 45, no. 8, pp. 1092–1097, Aug. 1998.

[62] B. Aiazzi, L. Alparone, S. Baronti, and F. Lotti, "Lossless image compression by quantization feedback in a content-driven enhanced Laplacian pyramid," *IEEE Trans. Image Process.*, vol. 6, no. 6, pp. 831–843, Jun. 1997.

[63] B. Aiazzi, L. Alparone, S. Baronti, G. Chirò, F. Lotti, and M. Moroni, "A pyramid-based error-bounded encoder: An evaluation on X-ray chest images," *Signal Process.*, vol. 59, no. 2, pp. 173–187, Jun. 1997.

[64] L. Gagnon and A. Jouan, "Speckle filtering of SAR images: a comparative study between complex-wavelet-based and standard filters," in *Wavelet Applications in Signal and Image processing V*, 1997, vol. 3169 of *Proc. of SPIE*, pp. 80–91.

[65] E. Hervet, R. Fjørtoft, P. Marthon, and A. Lopès, "Comparison of wavelet-based and statistical speckle filters," in *SAR Image Analysis, Modelling, and Techniques III*, F. Posa, Ed., 1998, vol. 3497 of *Proc. of SPIE*, pp. 43–54.

[66] M. Simard, G. DeGrandi, K. P. B. Thomson, and G. B. Bénié, "Analysis of speckle noise contribution on wavelet decomposition of SAR images," *IEEE Trans. Geosci. Remote Sens.*, vol. 36, no. 6, pp. 1953–1962, Nov. 1998.

[67] D. L. Donoho, "Denoising by soft-thresholding," *IEEE Trans. Inf. Theory*, vol. 41, no. 3, pp. 613–627, Mar. 1995.

[68] H. Guo, J. E. Odegard, M. Lang, R. A. Gopinath, I. W. Selesnick, and C. S. Burrus, "Wavelet based speckle reduction with application to SAR based ATD/R," in *Proc. IEEE Int. Conf. on Image Processing (ICIP)*, 1994, vol. 1, pp. 75–79.

[69] J. R. Sveinsson and J. A. Benediktsson, "Almost translation invariant wavelet transformations for speckle reduction of SAR images," *IEEE Trans. Geosci. Remote Sens.*, vol. 41, no. 510, pp. 2404–2408, Oct. 2003.

[70] Z. Zeng and I. Cumming, "Bayesian speckle noise reduction using the discrete wavelet transform," in *Proc. IEEE Int. Geoscience and Remote Sensing Symp. (IGARSS)*, 1998, vol. 1, pp. 7–9.

[71] H. Xie, L. E. Pierce, and F. T. Ulaby, "SAR speckle reduction using wavelet denoising and Markov random field modeling," *IEEE Trans. Geosci. Remote Sens.*, vol. 40, no. 10, pp. 2196–2212, Oct. 2002.

[72] A. Achim, P. Tsakalides, and A. Bezerianos, "SAR image denoising via Bayesian wavelet shrinkage based on heavy-tailed modeling," *IEEE Trans. Geosci. Remote Sens.*, vol. 41, no. 8, pp. 1773–1784, Aug. 2003.

[73] S. Solbø and T. Eltoft, "Homomorphic wavelet-based statistical despeckling of SAR images," *IEEE Trans. Geosci. Remote Sens.*, vol. 42, no. 4, pp. 711–721, Apr. 2004.

[74] M. I. H. Bhuiyan, M. O. Ahmad, and M. N. S. Swamy, "A new homomorphic Bayesian wavelet-based MMAE filter for despeckling SAR images," in *Proc. IEEE Int. Symp. on Circuits And Systems (ISCAS)*, May 2005, vol. 5, pp. 4935–4938.

[75] M. I. H. Bhuiyan, M. O. Ahmad, and M. N. S. Swamy, "Spatially adaptive wavelet-based method using the Cauchy prior for denoising the SAR images," *IEEE Trans. Circuits Syst. Video Technol.*, vol. 17, no. 4, pp. 500–507, Apr. 2007.

[76] A. Achim, E. E. Kuruoglu, and J. Zerubia, "SAR image filtering based on the heavy-tailed Rayleigh model," *IEEE Trans. Image Process.*, vol. 15, no. 9, pp. 2686–2693, Sep. 2006.

[77] S. Foucher, G. B. Bénié, and J.-M. Boucher, "Multiscale MAP filtering of SAR images," *IEEE Trans. Image Process.*, vol. 10, no. 1, pp. 49–60, Jan. 2001.

[78] F. Argenti and L. Alparone, "Speckle removal from SAR images in the undecimated wavelet domain," *IEEE Trans. Geosci. Remote Sens.*, vol. 40, no. 11, pp. 2363–2374, Nov. 2002.

[79] Min Dai, Cheng Peng, A.K. Chan, and D. Loguinov, "Bayesian wavelet shrinkage with edge detection for SAR image despeckling," *IEEE Trans. Geosci. Remote Sens.*, vol. 42, no. 8, pp. 1642–1648, Aug. 2004.

[80] R Touzi, A. Lopès, and P. Bousquet, "A statistical and geometrical edge detector for SAR images," *IEEE Trans. Geosci. Remote Sens.*, vol. 26, no. 6, pp. 764–773, Nov. 1988.

[81] S. Solbø and T. Eltoft, "Γ-WMAP: a statistical speckle filter operating in the wavelet domain," *Int. J. Remote Sens.*, vol. 25, no. 5, pp. 1019–1036, Mar. 2004.

[82] F. Argenti, T. Bianchi, and L. Alparone, "Multiresolution MAP despeckling of SAR images based on locally adaptive generalized Gaussian PDF modeling," *IEEE Trans. Image Process.*, vol. 15, no. 11, pp. 3385–3399, Nov. 2006.

[83] T. Bianchi, F. Argenti, and L. Alparone, "Segmentation-based MAP despeckling of SAR images in the undecimated wavelet domain," *IEEE Trans. Geosci. Remote Sens.*, vol. 46, no. 9, pp. 2728–2742, Sep. 2008.

[84] Ran Tao, Hui Wan, and Yue Wang, "Artifact-free despeckling of SAR images using contourlet," *IEEE Geosci. Remote Sens. Lett.*, vol. 9, no. 5, pp. 980–984, Sep. 2012.

[85] F. Argenti, T. Bianchi, A. Lapini, and L. Alparone, "Fast MAP despeckling based on Laplacian–Gaussian modeling of wavelet coefficients," *IEEE Geosci. Remote Sens. Lett.*, vol. 9, no. 1, pp. 13–17, Jan. 2012.

[86] Hongzhen Chen, Yueting Zhang, Hongqi Wang, and Chibiao Ding, "Stationary-wavelet-based despeckling of SAR images using two-sided generalized gamma models," *IEEE Geosci. Remote Sens. Lett.*, vol. 9, no. 6, pp. 1061–1065, Nov. 2012.

[87] Heng-Chao Li, Wen Hong, Yi-Rong Wu, and Ping-Zhi Fan, "Bayesian wavelet shrinkage with heterogeneity-adaptive threshold for SAR image despeckling based on generalized gamma distribution," *IEEE Trans. Geosci. Remote Sens.*, vol. 51, no. 4, pp. 2388–2402, Apr. 2013.

[88] A. Pižurica, W. Philips, I. Lemahieu, and M. Acheroy, "A versatile wavelet domain noise filtration technique for medical imaging," *IEEE Trans. Med. Imag.*, vol. 22, no. 3, pp. 323–331, Mar. 2003.

[89] S. Fukuda and H. Hirosawa, "Smoothing effect of wavelet-based speckle filtering: the Haar basis case," *IEEE Trans. Geosci. Remote Sens.*, vol. 37, no. 2, pp. 1168–1172, Mar. 1999.

[90] Y. Hawwar and A. Reza, "Spatially adaptive multiplicative noise image denoising technique," *IEEE Trans. Image Process.*, vol. 11, no. 12, pp. 1397–1404, Dec. 2002.

[91] L. Alparone, S. Baronti, and R. Carlà, "Two-dimensional rank-conditioned median filter," *IEEE Trans. Circuits Syst. II*, vol. 42, no. 2, pp. 130–132, Feb. 1995.

[92] L. Alparone, S. Baronti, R. Carlà, and C. Puglisi, "An adaptive order-statistics filter for SAR images," *Int. J. Remote Sens.*, vol. 17, no. 7, pp. 1357–1365, May 1996.

[93] T. R. Crimmins, "Geometric filter for speckle reduction," *Appl. Optics*, vol. 24, no. 10, pp. 1438–1443, May 1985.

[94] L. Alparone and A. Garzelli, "Decimated geometric filter for edge-preserving removal of non-white image noise," *Pattern Recogn. Lett.*, vol. 19, no. 1, pp. 89–96, Jan. 1998.

[95] P. Perona and J. Malik, "Scale-space and edge detection using anisotropic diffusion," *IEEE Trans. Pattern Anal. Mach. Intell.*, vol. 12, no. 7, pp. 629–639, Jul. 1990.

[96] Yongjian Yu and S. T. Acton, "Speckle reducing anisotropic diffusion," *IEEE Trans. Image Process.*, vol. 11, no. 11, pp. 1260–1270, Nov. 2002.

[97] Yongjian Yu and S. T. Acton, "Automated delineation of coastline from polarimetric SAR imagery," *Int. J. Remote Sens.*, vol. 25, no. 17, pp. 3423–3438, Sep. 2004.

[98] R. G. White, "A simulated annealing algorithm for SAR and MTI image cross section estimation," in *SAR Data Processing for Remote Sensing, 137*, 1994, vol. 2316 of *Proc. of SPIE*, pp. 339–360.

[99] I. McConnell and C. Oliver, "Comparison of annealing and iterated filters for speckle reduction in SAR," in *Microwave Sensing and Synthetic Aperture Radar, 74*, 1994, vol. 2958 of *Proc. of SPIE*, pp. 74–85.

[100] J. Schou and H. Skriver, "Restoration of polarimetric SAR images using simulated annealing," *IEEE Trans. Geosci. Remote Sens.*, vol. 39, no. 9, pp. 2005–2016, Sep. 2001.

[101] Jong-Sen Lee, "Digital image smoothing and the sigma filter," *Comput. Vis. Graph. Image Process.*, vol. 24, no. 2, pp. 255–269, Nov. 1983.

[102] Jong-Sen Lee, "A simple speckle smoothing algorithm for synthetic aperture radar images," *IEEE Trans. Syst., Man, Cybern.*, vol. SMC-13, no. 1, pp. 85–89, Jan. 1983.

[103] L. Alparone, S. Baronti, and A. Garzelli, "A hybrid sigma filter for unbiased and edge-preserving speckle reduction," in *Proc. IEEE Int. Geoscience and Remote Sensing Symp. (IGARSS)*, 1995, vol. 2, pp. 1409–1411.

[104] Jong-Sen Lee, Jen-Hung Wen, T. L. Ainsworth, Kun-Shan Chen, and A. J. Chen, "Improved sigma filter for speckle filtering of SAR imagery," *IEEE Trans. Geosci. Remote Sens.*, vol. 47, no. 1, pp. 202–213, Jan. 2009.

[105] C. Tomasi and R. Manduchi, "Bilateral filtering for gray and color images," in *Proc. 6th Int. Conf. on Computer Vision (ICCV)*, 1998, pp. 839–846.

[106] W. G. Zhang, Q. Zhang, and C. S. Yang, "Improved bilateral filtering for SAR image despeckling," *Electron. Lett.*, vol. 47, no. 4, pp. 286–288, Feb. 2011.

[107] Guang-Ting Li, Chun-Le Wang, Ping-Ping Huang, and Wei-Dong Yu, "SAR image despeckling using a space-domain filter with alterable window," *IEEE Geosci. Remote Sens. Lett.*, vol. 10, no. 2, pp. 263–267, Mar. 2013.

[108] C.-A. Deledalle, L. Denis, and F. Tupin, "Iterative weighted maximum likelihood denoising with probabilistic patch-based weights," *IEEE Trans. Image Process.*, vol. 18, no. 12, pp. 2661–2672, Dec. 2009.

[109] S. Parrilli, M. Poderico, C. V. Angelino, and L. Verdoliva, "A nonlocal SAR image denoising algorithm based on LLMMSE wavelet shrinkage," *IEEE Trans. Geosci. Remote Sens.*, vol. 50, no. 2, pp. 606–616, Feb. 2012.

[110] A. Buades, B. Coll, and J.-M. Morel, "A non-local algorithm for image denoising," in *Proc. IEEE Conf. on Computer Vision and Pattern Recognition (ICCVPR)*, 2005, vol. 2, pp. 60–65.

[111] K. Dabov, A. Foi, V. Katkovnik, and K. Egiazarian, "Image denoising by sparse 3-D transform-domain collaborative filtering," *IEEE Trans. Image Process.*, vol. 16, no. 8, pp. 2080–2095, Aug. 2007.

[112] T. Teuber and A. Lang, "A new similarity measure for nonlocal filtering in the presence of multiplicative noise," *Comput. Stat. Data An.*, vol. 56, no. 12, pp. 3821–3842, Dec. 2012.

[113] C. Kervrann, J. Boulanger, and P. Coupé, "Bayesian non-local means filter, image redundancy and adaptive dictionaries for noise removal," in *Proc. 1st Int. Conf. on Scale Space and Variational Methods in Computer Vision (SSVM)*, 2007, pp. 520–532.

[114] P. Coupe, P. Hellier, C. Kervrann, and C. Barillot, "Bayesian non local means-based speckle filtering," in *5th IEEE Int. Symp. on Biomedical Imaging: From Nano to Macro*, 2008, pp. 1291–1294.

[115] Hua Zhong, Yongwei Li, and Lc Jiao, "SAR image despeckling using Bayesian nonlocal means filter with sigma preselection," *IEEE Geosci. Remote Sens. Lett.*, vol. 8, no. 4, pp. 809–813, Jul. 2011.

[116] D. Gragnaniello, G. Poggi, and L. Verdoliva, "Classification-based non-local SAR despeckling," in *Proc. Tyrrhenian Workshop on Advances in Radar and Remote Sensing*, 2012, pp. 121–125.

[117] L. I. Rudin, S. Osher, and E. Fatemi, "Nonlinear total variation based noise removal algorithms," *Physica D*, vol. 60, no. 1–4, pp. 259–268, Nov. 1992.

[118] L. I. Rudin, P.-L. Lions, and S. Osher, "Multiplicative denoising and deblurring: theory and algorithms," in *Geometric Level Set Methods in Imaging, Vision, and Graphics*, pp. 103–119. Springer, New York, 2003.

[119] G. Aubert and J. Aujol, "A variational approach to removing multiplicative noise," *SIAM J. Appl. Math.*, vol. 68, no. 4, pp. 925–946, Dec. 2008.

[120] Jianing Shi and S. Osher, "A nonlinear inverse scale space method for a convex multiplicative noise model," *SIAM J. Imaging Sci.*, vol. 1, no. 3, pp. 294–321, Sep. 2008.

[121] Yu-Mei Huang, Michael K. Ng, and You-Wei Wen, "A new total variation method for multiplicative noise removal," *SIAM J. Imaging Sci.*, vol. 2, no. 1, pp. 20–40, Jan. 2009.

[122] S. Durand, J. Fadili, and M. Nikolova, "Multiplicative noise removal using L1 fidelity on frame coefficients," *J. Math. Imaging Vis.*, vol. 36, no. 3, pp. 201–226, Mar. 2010.

[123] G. Steidl and T. Teuber, "Removing multiplicative noise by Douglas-Rachford splitting methods," *J. Math. Imaging Vis.*, vol. 36, no. 2, pp. 168–184, Feb. 2010.

[124] J. M. Bioucas-Dias and M. A. T. Figueiredo, "Multiplicative noise removal using variable splitting and constrained optimization," *IEEE Trans. Image Process.*, vol. 19, no. 7, pp. 1720–1730, Jul. 2010.

[125] L. Denis, F. Tupin, J. Darbon, and M. Sigelle, "SAR image regularization with fast approximate discrete minimization," *IEEE Trans. Image Process.*, vol. 18, no. 7, pp. 1588–1600, Jul. 2009.

[126] F. Palsson, J. R. Sveinsson, M. O. Ulfarsson, and J. A. Benediktsson, "SAR image denoising using total variation based regularization with SURE-based optimization of the regularization parameter," in *Proc. IEEE Int. Geoscience and Remote Sensing Symp. (IGARSS)*, 2012, pp. 2160–2163.

[127] D. Gleich and M. Kseneman, "A comparison of regularization-based methods for despeckling of SLC SAR images," in *Proc. 9th European Conf. on Synthetic Aperture Radar (EUSAR)*, 2012, pp. 784–787.

[128] D. L. Donoho, "Compressed sensing," *IEEE Trans. Inf. Theory*, vol. 52, no. 4, pp. 1289–1306, Apr. 2006.

[129] S. Foucher, "SAR image filtering via learned dictionaries and sparse representations," in *Proc. IEEE Int. Geoscience and Remote Sensing Symp. (IGARSS)*, 2008, vol. I, pp. 229–232.

[130] M. Yang and G. Zhang, "SAR image despeckling using over-complete dictionary," *Electron. Lett.*, vol. 48, no. 10, pp. 596–597, May 2012.

[131] Yan Hao, Xiangchu Feng, and Jianlou Xu, "Multiplicative noise removal via sparse and redundant representations over learned dictionaries and total variation," *Signal Process.*, vol. 92, no. 6, pp. 1536–1549, Jun. 2012.

[132] R. Coifman and D. L. Donoho, "Translation-invariant de-noising," in *Wavelets and Statistics*, A. Antoniadis, Ed., Lecture Notes. Springer-Verlag, Berlin, Heidelberg, New York, 1995.

[133] F. Argenti, T. Bianchi, A. Lapini, and L. Alparone, "Bayesian despeckling of SAR images based on Laplacian–Gaussian modeling of undecimated wavelet coefficients," in *Proc. IEEE Int. Conf. on Acoustics, Speech and Signal Processing (ICASSP)*, 2011, pp. 1445–1448.

[134] H. Rabbani, M. Vafadust, P. Abolmaesumi, and S. Gazor, "Speckle noise reduction of medical ultrasound images in complex wavelet domain using mixture priors," *IEEE Trans. Biomed. Eng.*, vol. 55, no. 9, pp. 2152–2160, Sep. 2008.

[135] Zhou Wang, A. C. Bovik, H. R. Sheikh, and E. P. Simoncelli, "Image quality assessment: from error visibility to structural similarity," *IEEE Trans. Image Process.*, vol. 13, no. 4, pp. 600–612, Apr. 2004.

[136] F. Sattar, L. Floreby, G. Salomonsson, and B. Lovstrom, "Image enhancement based on a nonlinear multiscale method," *IEEE Trans. Image Process.*, vol. 6, no. 6, pp. 888–895, Jun. 1997.

[137] T. Bianchi, F. Argenti, A. Lapini, and L. Alparone, "Amplitude vs intensity despeckling in the wavelet domain using Bayesian estimators," in *Proc. Tyrrhenian Workshop on Advances in Radar and Remote Sensing*, 2012, pp. 267–274.

[138] G. R. Benitz, "High-definition vector imaging," *Lincoln Lab. J.*, vol. 10, no. 2, pp. 147–170, 1997.

[139] M. Çetin, W. C. Karl, and D. A. Castañon, "Evaluation of a regularized SAR imaging technique based on recognition-oriented features," in *Algorithms for Synthetic Aperture Radar Imagery VII*, 2000, vol. 4053 of *Proc. of SPIE*, pp. 40–51.

[140] A. Lapini, T. Bianchi, F. Argenti, and L. Alparone, "Blind whitening of correlated speckle to enforce despeckling of single-look high-resolution SAR images," in *Image and Signal Processing for Remote Sensing XVIII*, 2012, vol. 8537 of *Proc. of SPIE*, pp. 85370Z–85370Z–8.

[141] A. Lapini, T. Bianchi, F. Argenti, and L. Alparone, "Blind speckle decorrelation for SAR image despeckling," *IEEE Trans. Geosci. Remote Sens.*, Article in Press.

[142] B. Aiazzi, L. Alparone, F. Argenti, S. Baronti, T. Bianchi, and A. Lapini, "An experimental setup for multiresolution despeckling of COSMO-SkyMed image products," in *SAR Image Analysis, Modeling, and Techniques XII*, 2011, vol. 8536 of *Proc. of SPIE*, pp. 853603–853603–6.

[143] T. Bianchi, F. Argenti, A. Lapini, and L. Alparone, "Amplitude vs intensity Bayesian despeckling in the wavelet domain for SAR images," *Digit. Signal Process.*, Article in Press.

[144] B. Aiazzi, L. Alparone, F. Argenti, S. Baronti, T. Bianchi, and A. Lapini, "An unsupervised method for quality assessment of despeckling: an evaluation on COSMO-SkyMed data," 2011, vol. 8197 of *Proc. of SPIE*, pp. 81790D–81790D–10.

[145] B. Aiazzi, L. Alparone, S. Baronti, A. Garzelli, and C. Zoppetti, "Nonparametric change detection in multitemporal SAR images based on mean-shift clustering," *IEEE Trans. Geosci. Remote Sens.*, vol. 51, no. 4, pp. 2022–2031, Apr. 2013.